Synthesis and Characterization of Second- Generation Iron Pro-chelators

by

Lissette Perez

Department of Chemistry
Duke University

Date:_____
Approved:

_____
Katherine J. Franz, Supervisor

_____
Alvin Crumbliss

_____
Richard MacPhail

Thesis submitted in partial fulfillment of
the requirements for the degree of Master of Science in the Department of Chemistry in the Graduate School
of Duke University

2010

ABSTRACT

Synthesis and Characterization of Second- Generation Iron Pro-chelators

by

Lissette Perez

Department of Chemistry
Duke University

Date:_____
Approved:

_____
Katherine J. Franz, Supervisor

_____
Alivn Crumbliss

_____
Richard MacPhail

An abstract of a thesis submitted in partial
fulfillment of the requirements for the degree
of Master of Science in the Department of
Chemistry in the Graduate School
of Duke University

2010

Abstract

Excessive amounts of labile metals such as iron, zinc, and copper have been found in the brains of patients diagnosed with various neurodegenerative diseases, which include Alzheimer's and Parkinson's disease. Iron and copper can participate in the Haber-Weiss cycle forming reactive oxygen species, ROS, which can induce cell death. *In vivo*, these labile metals act catalytically regenerating additional ROS.

It has recently become evident that these neurodegenerative diseases are complex and have various targets for therapy. Described herein are the newest approaches to tackling those multifaceted issues using multifunctional chelators as well as an in depth look at a specific class of iron binding pro-chelators. Researchers have taken advantage of properties that increase cell and blood brain barrier, BBB, permeability, increase antioxidant capabilities, increased selectivity for metals in damage prone environments, lower Aβ peptide aggregation, and inhibit key enzymes associated with disease pathways.

Our research group has described sets of masked chelators, which have the potential for selectivity binding iron and copper in damage prone environments. QBP, a hydroxyquinoline-based pro-chelator was recently shown to inhibit further Aβ aggregation and diminish copper's reactivity while BSIH, a salicylaldhyde isonicotinic hydrazone pro-chelator, has been shown to react selectively with hydrogen peroxide revealing an active chelator able to bind iron. Described in this thesis is a set of iron pro-chelator derivatives of the parent compound, BSIH. These masked chelators can potentially reveal high affinity metal ligands when oxidized by H_2O_2. Unlike traditional iron chelators, which can disrupt iron homeostasis, these pro-chelators have a protective mask consisting of various boronic esters that react and reveal a phenolic oxygen

selectively by H_2O_2. Studies on kinetics of oxidation by H_2O_2, solubility, iron affinity, and stability in various conditions have been established.

Contents

List of Tables

List of Figures

Schemes

1. Minding Metals: Tailoring multifunctional chelating agents for neurodegenerative diseases[†]

1.1 Introduction

Iron, copper, and zinc play complicated roles in human health and disease. While all three are essential nutrients utilized as various protein cofactors, their misappropriation within cells and tissues can lead to significant damage. Biological systems tightly regulate these metals at both the systemic level of absorption and distribution as well as the cellular level of storage, recycling, and utilization so that the organism meets metabolic demand without over accumulation (for recent reviews of iron, copper, and zinc homeostasis see references[1-3]). Excess metal that is not appropriately contained by the proteins or vesicles that utilize, store, or transport it becomes available for unintentional and potentially toxic reactivity. One of the dangers of redox-active metals like iron and copper is their ability to promote the formation of highly toxic hydroxyl radicals that oxidize biomolecules and subsequently lead to cell death.[4, 5] Even in the absence of redox activity, metal cations like Zn^{2+} and Cu^{2+} may also cause damage by inducing aberrant protein aggregation.[6, 7]

Both kinds of metal-promoted damage, oxidative stress and protein misfolding, have been linked to Parkinson's, Alzheimer's, and other neurodegenerative diseases.[8-13] Furthermore, there is increasing recognition that these diseases are associated with localized accumulation of metal ions in disease-affected regions.[14] Iron-induced oxidative stress in particular is speculated to play a role in a wide variety of progressive inflammatory and degenerative diseases, ranging from atherosclerosis and aging to diabetes and macular degeneration.[15] The emphasis here is on *localized* misregulation, as

---

[†]Chapter 1 is a slightly modified version of a review recently been published in Dalton Transactions. L.R. Perez and K.J. Franz, Dalton Transactions 2010, 39, 2177-2187

these diseases are not characterized by systemic metal imbalances, as is the case with traditional iron overload diseases like hemochromatosis and thalassemia.

Inhibiting metal-promoted damage by using small molecule chelating agents is a promising strategy for treating diseases associated with localized metal accumulation.[10, 16-18] The target pool of metal ions in these diseases, however, is significantly different from diseases of systemic metal overload where the target metal is plentiful and more readily available for sequestration. Furthermore, our current understanding of metal homeostasis in the central nervous system is limited, which further constrains the interpretation of the effects of manipulating metals in the brain.[19] Designing chelators to target localized metal imbalance therefore presents unique challenges. Generalized metal chelation can indeed protect against acute oxidative stress or inhibit protein aggregation, but long-term treatment with metal chelators poses serious risks associated with depletion or redistribution of healthy metal ions, inhibition of metalloenzymes, or other unintended consequences.

Research on medicinal iron chelators over the last 40 years has been dominated by the search for alternatives to desferrioxamine B (DFO, see **Figure 1**), the naturally occurring siderophore that has been used clinically since the 1970s for treating transfusional iron overload diseases.[20] DFO is a hydrophilic, hexadentate chelator that is not absorbed by the gut and has a short plasma half-life, requiring it to be administered daily in large doses via subcutaneous transfusion. Extensive research to identify alternatives has lead to the commercial development of two orally available agents, the bidentate hydroxypyridinone known as L1 or deferiprone, and the tridententate chelator deferasirox, or Exjade (**Figure 1**).[21-23] The targets of all these drugs are primarily non-transferrin bound iron in the plasma, followed by intracellular iron stores in the liver, heart and endocrine tissues.

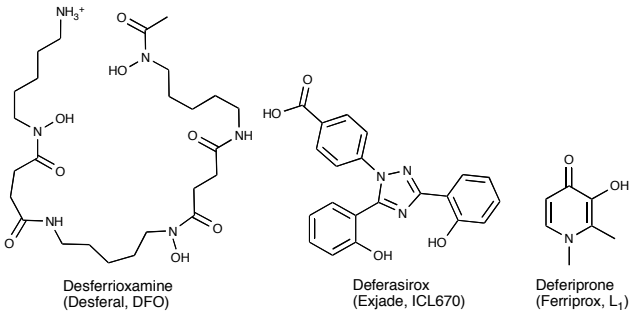

Figure 1: Structures of select medicinal iron chelators.

While chelating agents developed for systemic iron overload diseases are feasible starting points for developing agents for localized metal imbalance, the variation in the target metal pools requires chelators with different chemical properties. For example, avoiding chelator access to the brain is critical for transfusional iron overload, whereas crossing the blood–brain barrier (BBB) is obligatory for treating neurodegeneration. DFO is not a reasonable candidate due to its inability to cross membranes. While increasing the lipophilicity of a chelator may improve BBB penetration, this same property will also improve general intracellular access where it can inhibit essential non-heme iron enzymes like ribonucleotide reductase, lipoxygenase and tyrosine hydroxylase.[24, 25] For example, deferiprone crosses the BBB, but it also inhibits catechol-*O*-methyltransferase and tyrosine and tryptophan hydroxylases by forming ternary complexes with iron in the enzyme active site.[26] Tyrosine hydroxylase is a critical enzyme for synthesis of the key neurotransmitter dopamine, therefore its inhibition is undesirable in Parkinson's patients.

For localized metal overload, an optimal chelator needs to readily pass cellular membranes, specifically sequester only that fraction of metal that is causing damage without depleting healthy metal stores, form non redox-active complexes that also pass

cellular membranes for elimination, avoid redistribution of iron or other metals within a cell or between cells, and be non-toxic.

It is now becoming apparent that the next generation of therapeutically relevant metal chelators must have multiple functions to be most effective. Some noteworthy advances in these multifunctional metal chelating agents involve functions that increase cell and BBB permeability, increase anti-oxidant capabilities, increase selectivity for metals in damage-prone environments, lower Aβ peptide aggregation, and inhibit key enzymes associated with specific disease pathways. Chapter one will highlight recent advances and clever strategies in the design of multifaceted metal chelating agents targeted against neurodegenerative disease. Chapter two of this document will focus more specifically on masked iron pro-chelators, which are activated in the presence of H_2O_2.

1.2 Increasing uptake into cells and across the blood brain barrier

If metal chelating agents are to be used to treat neurodegenerative disease, a prerequisite is that they must bypass the blood–brain barrier, a continuous layer of endothelial cells connected by tight junctions where the bloodstream meets the neural tissue.[13] Its function is to restrict high molecular weight compounds and most ions from entering the brain while allowing essential nutrients to pass through, thereby blocking entry of neurotoxic materials while minimizing fluctuations in levels of vital substances in the central nervous system. As mentioned previously, abnormally elevated levels of metals have been found localized in the brains of patients with neurodegenerative diseases.[14] In order to sequester potentially damaging sources of aberrant metal ions, chelating agents must be able to pass through the BBB; however, creating a compound capable of permeating the BBB is not trivial. Conventional wisdom posits that the

molecule must be small (<500 Da), hydrophobic enough to diffuse passively through the membrane, yet hydrophilic enough to stay soluble in physiological environments.[13] Several strategies have been employed to overcome these obstacles, including linking carbohydrates, peptides, and nanoparticles to chelators to facilitate entry into cells.

1.2.1 Multifunctional agents that target specific transporters or receptors

1.2.1.1 Carbohydrate conjugates to facilitate BBB uptake

The brain consumes a significant amount of glucose and needs a mechanism that quickly passes it through the BBB to meet this need.[27] The high concentration of glucose transporters (GLUTs) at the BBB therefore provides an appealing pathway for drug delivery if the drug can be tagged with glucose moieties to facilitate GLUT-mediated transport. Orvig and coworkers have reported several glucose–chelator conjugates with this premise in mind. The multifunctional conjugates are based on tetrahydrosalen or hydroxypyridinone families of ligands that are decorated with glucose molecules, as shown in **Figure 2**.[27-30]

Using carbohydrates as the actual metal binding moiety poses a challenge since typical carbohydrates have problematic stereochemistry and bind weakly to metals.[31] The carbohydrate tag is instead installed as a pendant moiety onto a metal-binding ligand. In the first-generation tetrahydrosalen glucoconjugates (as in **1**, **Figure 2**), the sugar tags are on the outer rim of the chelator where they do not interfere with the metal-binding core. In later-generation hydroxypyridinone and tetrahydrosalen glucoconjugates (**2, 3** in **Figure 2**), the glucose appendages mask the metal binding site, which has the advantage of preventing systemic metal binding prior to enzymatic cleavage of the sugar. The glucose modification has been found to increase water

solubility, minimize toxicity, and shows promise for specific targeting of these compounds.[27, 30]

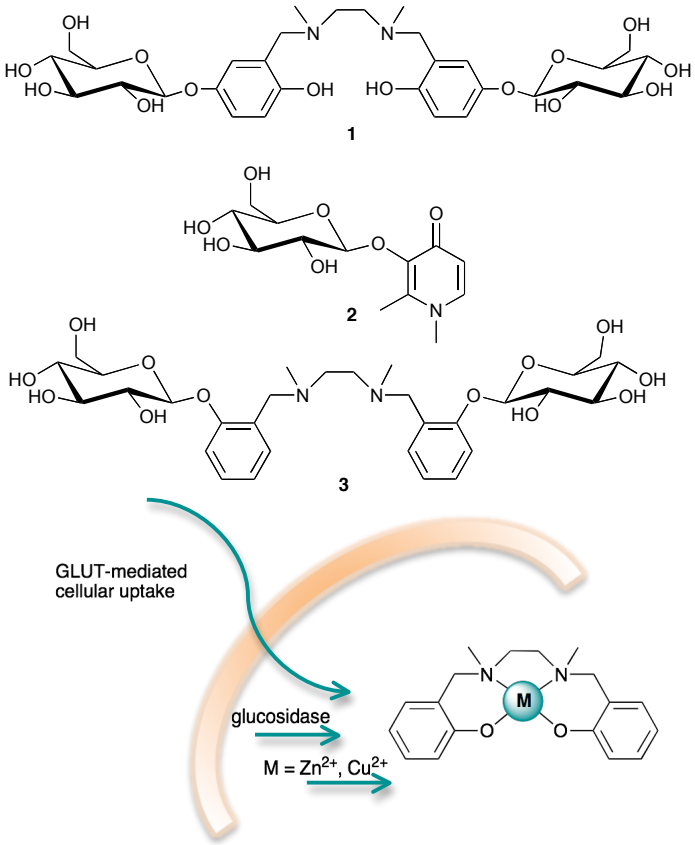

Figure 2: Top: structures of metal ion chelators containing pendant or masking carbohydrate groups. Bottom: schematic example of cellular uptake by glucose transporters of prochelator 3, followed by intracellular enzymatic activation and metal binding.

In vivo, these glucoconjugate pro-ligands are anticipated to gain entry into the brain via glucose transporters on the surface of endothelial cells on the BBB.[27] Once inside cells, the glucose masking group would be enzymatically cleaved to release the active chelating agent, as shown at the bottom of **Figure 2**. As a proof-of-principle, it was shown that both a broad-spectrum glucosidase from *Agrobacterium faecalis* and a rat brain homogenate as a model of glucosidase activity convert the glucoconjugate prochelators into their metal-binding hydroxypyridinone or tetrahydrosalen versions.[28, 30]

A rat brain perfusion experiment with a radiolabeled hydroxypryidinone glucoconjugate demonstrated adequate cerebral uptake, showing that these compounds are indeed taken across the BBB.[28]

Once the carbohydrate groups are cleaved by β-glucosidases, the released tetrahydrosalen or hydroxypyridinone chelators are available to bind metals. In addition, both classes of compounds are effective radical-scavenging antioxidants.[28, 29] *In vitro* studies show that both chelators compete with amyloid-beta (Aβ) peptides for binding Cu^{2+} and Zn^{2+}, and decrease $A\beta_{1-40}$ peptide aggregation induced by these metals.[27-30] The ability of **1** to prevent Aβ peptide aggregation was comparable to that of EDTA despite its lower affinity for Cu^{2+}. This observation could be attributed to the increased lipophilicity and/or intercalating ability of the tetrahydrosalen compound into Aβ peptide aggregates.[30]

1.2.1.2 Iron binding peptides that target neuronal receptors

Functionalizing neuropeptides with metal chelating groups is another strategy to target agents to specific brain locations.[32] Vasoactive intestinal peptide, VIP, is widely distributed in areas of the brain associated with learning and memory and is associated with specific neuronal receptors in the brain.[33] An eight amino acid peptide abbreviated as NAP with amino acid sequence Asn-Ala-Pro-Val-Ser-Ile-Pro-Gln is the smallest active portion of activity-dependent neuroprotective protein, ADNP, which is a glial cell mediator of VIP-induced neuroprotection.[32] NAP has demonstrated potent neuroprotection in both cell culture and animal models of neurodegeneration and is capable of crossing the BBB.[34] In order to create a multifunctional agent that would take advantage of the targeting ability of the NAP neuropeptide to sites of neurodegeneration and expand its antioxidant potential, Fridkin and coworkers modified the native peptide by adding hydroxamate (**4**) or 8-hydroxyquinoline (**5**)

moieties to derivatives of NAP, as shown in **Figure 3**.[32, 34] The modified peptides form stable metal ion complexes with $Fe^{2+/3+}$, Cu^{2+} and Zn^{2+} in water, pH 5–7, whereas the parent NAP peptide shows no binding affinity to these metal ions. The peptides containing two hydroxamate units inhibit lipid peroxidation and iron-catalyzed hydroxyl radical formation *in vitro* and protect neuroblastoma cells against oxidative stress induced by exogenous hydrogen peroxide.[34] Although not yet tested, these peptides could allow for transport and localization of therapeutic chelators into the brain.

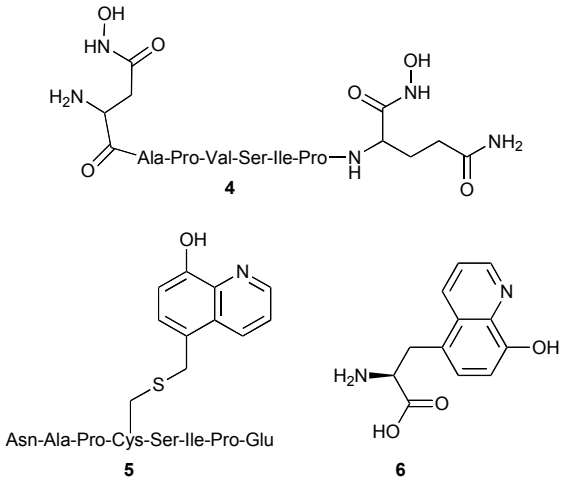

Figure 3: Neuroprotective NAP peptides modified with bis-hydroxamic acid (4) or hydroxyquinoline (5) groups; and amino acid derivative of 8-hydroxyquinoline (6).

An alternative strategy for targeting chelators into the brain is to modify them with a neutral amino acid carrier group that would facilitate uptake by system L, a known brain uptake pathway for hydrophilic amino acids including L-DOPA. Fridkin and coworkers therefore synthesized and studied a bifunctional iron chelator, M10 (**6**), that fuses an 8-hydroxyquinoline unit with an alanine amino acid, as shown in **Figure 3**.[35] They have shown that **6** is a metal chelator that exibits free radical scavenging properties and is water soluble. The hydrophilicity of **6** may prevent its passive diffusion into cells, which would avert its interference with normal, systemic metal

metabolism. It is hoped that the carrier group would thus allow selective targeting of the agent into the brain while minimizing effects on systemic metal balance.[35]

1.2.1.3 Chelators with moieties that target integrin receptors

Overexpression of the cell surface a_vb_3 integrin receptor (ABIR) has been found on activated endothelial cells in the neovasculature of tumors and has been associated with tumor growth, invasion, and metastasis.[36] Fluorescent probes and anticancer agents have previously been shown to be taken up when coupled to ABIR-binding peptides.[37, 38] In order to use this approach to improve the uptake of metal chelators, Achilefu and coworkers synthesized a tri-functional agent consisting of a DFO chelating unit, a near-infrared cypate fluorescent probe, and a cyclic RGD peptide that is known to bind the integrin receptor. The multifunctional molecule (**7**) is shown in **Figure 4**.

They found that the ABIR-avid RGD peptide improved the cellular internalization of the DFO analogue without permeating the cell nucleus, which can be damaging to the cell.[36] While this bioconjugate is not directed at a brain-specific receptor, the strategy shows that receptor-specific peptides can improve cellular uptake of metal chelators that otherwise have limited cellular access.

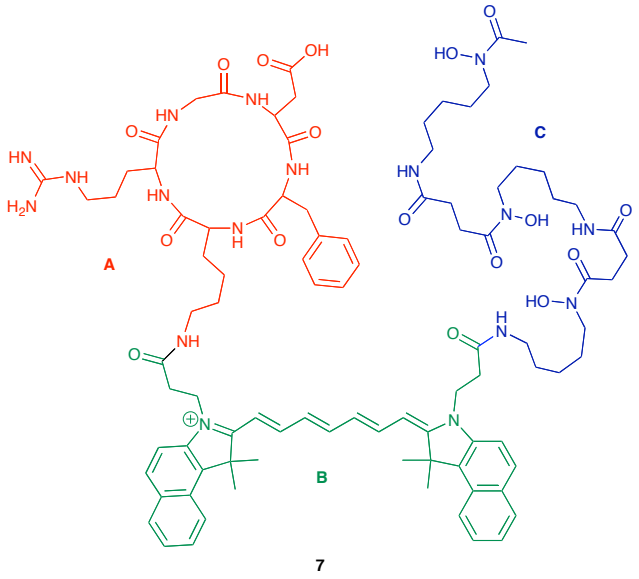

Figure 4: A trifunctional chelator composed of: (A) an ABIR-binding peptide to facilitate entry through cell membranes, (B) cypate as a near-IR probe for detection, and (C) DFO as the iron chelator.[36]

1.2.1.4 Nanoparticles as chelator carriers

Nanoparticles have been found to cross the BBB by receptor-mediated transport systems through brain endothelial cells and have shown promise in drug delivery.[39] This strategy is being pursued as a means to transport metal chelators into the brain. Mumper and coworkers coupled the Cu(I) chelator D-penicillamine, an FDA approved drug used to treat Wilson's disease patients, to nanoparticles by a disulfide bond, as shown in **8, Figure 5**.[40] The nanoparticles used for the chelator conjugates, which were composed of emulsifying wax and surfactants, had been previously found to cross the BBB with no effect on cerebral perfusion flow or BBB integrity and permeability in an *in situ* rat brain perfusion model.[40] The D-penicillamine, found to be highly hydrophobic on its own, was released from the nanoparticles when exposed to reducing conditions and was able to solublize copper-Aβ peptide aggregates *in vitro*.[40]

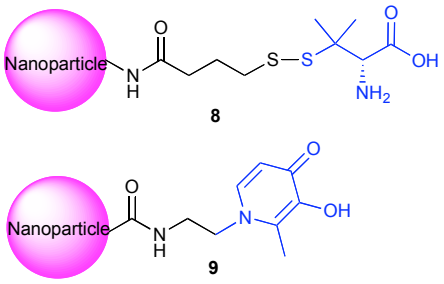

Figure 5: Nanoparticle carriers for penicillamine (8) and deferiprone (9) analogues.

With a similar concept in mind, Smith and coworkers devised polystyrene nanoparticles decorated with pyridinone chelators, as shown for Nano-N2PY, **9**, in **Figure 5**.[41, 42] In this case, conjugation of the chelators to the nanoparticle does not alter its metal chelating ability. The Nano-N2PY conjugates were shown to inhibit Aβ aggregation *in vitro* and to protect neuronal cells from Aβ -associated neurotoxicity.[42]

1.2.2 Strategies for increasing passive diffusion

1.2.2.3 Metal chelators with increased lipophilicity

Synthetic derivatives of the well-known siderophore, ferrichrome, have been shown to bind Fe^{3+} with a tris hydroxamate binding site and display no toxic properties in cell studies *in vitro*. Cabantchik and Shanzer presented a new class of lipophilic ferrichrome analogues containing acetoxymethyl ester moieties, (**10**) **Figure 6**.[43] The acetoxymethyl moieties provide the ferrichrome analogue with a hydrophobic region that facilitates entry of the chelator into cells. Once inside the cell, these molecules become hydrophilic by esterase-mediated hydrolysis of the acetoxymethyl groups. The R group on the tripodal anchor can be modified, allowing fluorescent labeling of the compound. Once the carboxylic acid groups are exposed, the diffusion of the chelator out of the cell is delayed when compared to a control containing stable ethyl ester groups instead of labile ester groups.[43]

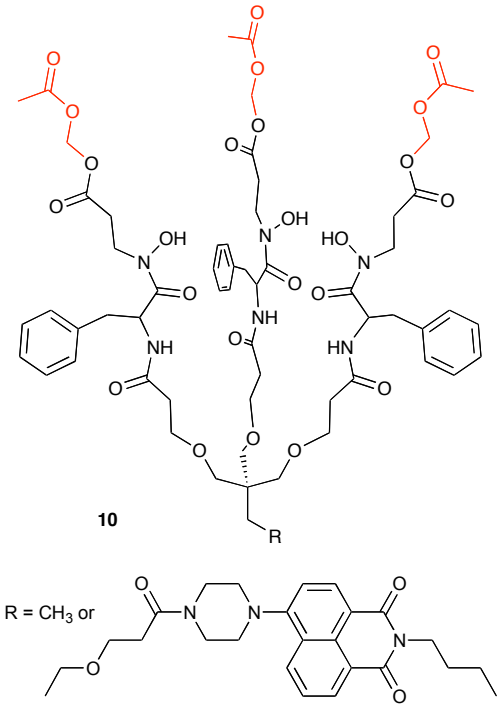

Figure 6: Acetoxymethyl protecting groups (highlighted in red) provide a lipophilic ferrichrome analogue (10) that is converted to a hydrophilic version (black) by intracellular esterases.[43]

In another strategy aimed at improving the lipophilicity of iron chelators, Shanzer and colleagues prepared a tris-hydroxamate chelator, **11** in **Figure 7**, wherein an isopentyl group that has been shown to assist in membrane crossing is used to anchor two ligand arms that contain hydroxamate chelating units.[44] In order to attain the proper octahedral geometry required for iron binding, one of the two arms contains an additional hydroxamate that is properly oriented for metal chelation by judicious incorporation of a proline residue. One of the analogs protects oligodendritic cells exposed to excess iron and H_2O_2 with a 25-fold increase in protection compared to DFO.[44] Future studies will consist of improving the lipophilicity of the analogues to improve the chelators activity.

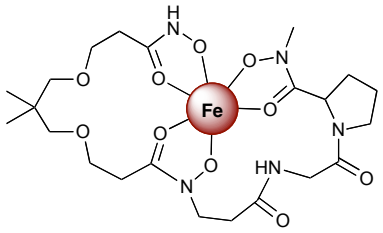

11

Figure 7: Tris-hydroxamate iron chelator (11) with a dipodal anchor to assist in crossing the cell membranes.[44]

1.3 Prochelators for triggered activation against oxidative stress

A leading hypothesis for the cause of cell death in degenerative disease is an increase in oxidative stress that results when reactive oxygen species (ROS) overwhelm the cell's inherent antioxidant mechanisms and damage cellular components.[13, 14] Oxidative stress results primarily from the highly reactive hydroxyl radical, $OH^{\bullet}$, formed by the oxidation of Fe^{2+} to Fe^{3+} by H_2O_2, the Fenton reaction, shown in **Scheme 1**.[4, 45] The iron can be catalytic if its coordination environment favors redox cycling and cellular reductants can reduce Fe^{3+} to Fe^{2+}. Iron-promoted oxidative stress may therefore be a critical component in diseases where normal iron homeostasis is impaired or where aberrant iron accumulation occurs.[46-49] The premise for using chelators to thwart oxidative stress is to sequester any "free" iron capable of undergoing this redox cycle into unreactive complexes to prevent further free radical production. The challenge for using chelating agents for these diseases is developing agents that are selective only for the harmful metal without disturbing healthy metal balance. The following examples show how selectivity can be achieved by reactivity of the chelating agent itself.

Scheme 1. The catalytic cycle of Fenton Chemistry

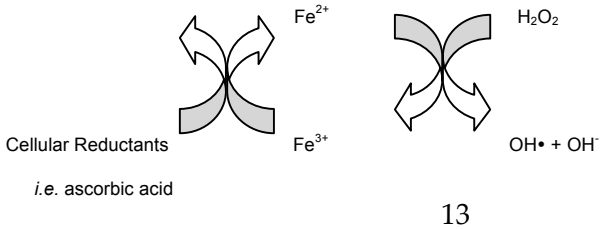

1.3.1 Selectivity based on chelator reactivity

1.3.1.1 Masked iron chelators

In 2006 our research group introduced a pro-chelator strategy that takes advantage of the reactivity associated with oxidative stress to generate metal chelators *in situ* to inhibit further oxidative damage.[50-52] This concept will be further discussed in chapter two of this document.

1.3.1.2 Photo-caged iron chelators

An alternative strategy for masking a chelating unit is to block metal binding with a photoactive protecting group to create a photo-caged chelator.[53] Exposure of UVA radiation to skin cells has been found to cause an immediate release of labile iron that exacerbates oxidative damage.[54] Pourzand and coworkers therefore prepared caged iron chelators that are activated when irradiated with UVA light.[53] Aroyl hydrazone chelators SIH, PIH and derivatives of the two were masked with ortho-nitrobenzyl protecting groups that prevent metal binding, as shown in **13** in **Figure 8**. Exposure to physiologically relevant levels of UVA light cause release of the active chelator. The caged compounds were found to be lipophilic enough to enter cells and exhibited no cytotoxic effects. Of the prochelators analyzed, 2-NPE-SIH (**13**) showed the most promise as a sunscreen component exhibiting protection at 500 kJ/m^2, the highest UVA dosage administered.[53]

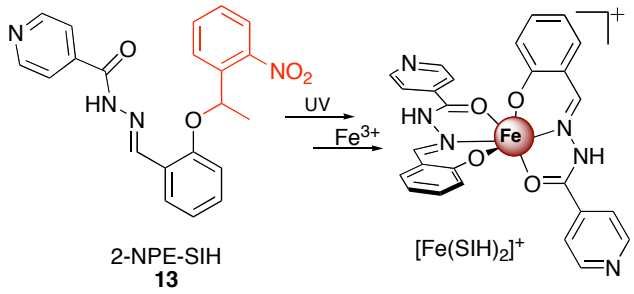

Figure 8: Exposure to UVA light induces release of the photoactive protecting group (colored in red) on 13 to generate the active chelator SIH available for metal binding.

1.3.1.3 Iron chelators activated by hydroxyl radicals

In another example where the reactivity of a chelating unit can be used as a switch to prevent further Fenton reactivity, Galey and coworkers showed that aminocarboxylate ligands with relatively weak iron affinity can be converted to high-affinity chelators under oxidative stress conditions. An example is shown in **Figure 9**. The compounds contain aromatic rings that are readily attacked by hydroxyl radicals generated at the iron center to produce phenolates that are well positioned to coordinate iron.[55-58] Thus under pro-oxidant conditions, *i.e.* H_2O_2 and a reductant, metal complexes like **14** are hydroxylated and their iron affinity increases. In addition to an increase in affinity, another consequence of the added phenolate donor is a decrease in Fe^{3+}/Fe^{2+} redox potential that prevents further redox cycling of iron.[56] The early compounds were not efficient at protecting cells from oxidative stress, probably because they were unable to cross cell membranes. Altering functional groups on the aromatic rings and esterifying the carboxylic acid groups alleviated this problem.[57] Non-specific esterases presumably cleave the esters intracellularly to give the active prochelator, which was found to protect skin fibroblasts against H_2O_2 toxicity with an IC_{50} of 3 μM.[57]

Similarly, Naughton and coworkers studied the potential radical scavenging of EDTA bis-(ethyl phenylalainate), EBEP, **15** in **Figure 9**.[59] In the presence of H_2O_2 and low concentrations of ascorbate, the oxidation products, *p*-, *o*-, and *m*- tyrosine are

obtained. However, the phenolate in the *o*- position is then the only one that can participate in intramolecular iron binding.

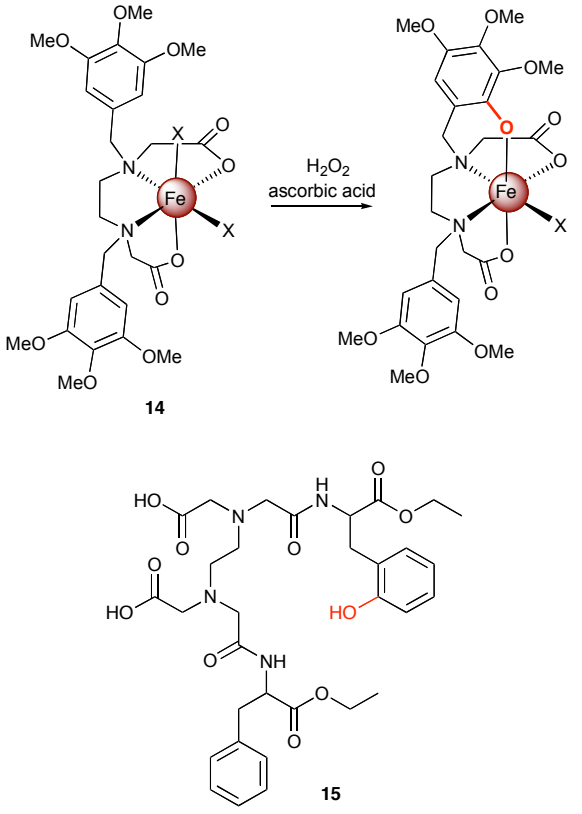

Figure 9: The tetradentate aminocarboxylate 14 binds iron weakly, but increases affinity following hydroxylation (highlighted in red) in the presence of H_2O_2 and a reductant. [X= coordinating solvent]. In a similar fashion, the aromatic rings in 15 can also be hydroxylated. In this case, only modifications at the ortho positions (highlighted in red) result in compounds with improved iron affinity.

1.4 Chelator–antioxidant hybrid molecules

1.4.1 L-DOPA/antioxidant hybrid molecules

Although many advances have been made in the area of Parkinson's Disease therapy, currently available drugs only treat the symptoms of the disease and can neither reverse nor slow its progression. The most clinically useful drug is still L-DOPA (3-hydroxyphenylalanine), a brain-accessible precursor to the neurotransmitter dopamine.[60] However, there are significant disadvantages to L-DOPA, beginning with

its poor bioavailability and susceptibility to chemical and enzymatic degradation. Moreover, L-DOPA has pro-oxidant properties that generate free radicals as a result of its autoxidation, which is accelerated in the prescence of iron or copper. In order to improve its bioavailability and provide a slow release mechanism for L-DOPA administration, several prodrug strategies have been evaluated.[61] As one example, Di Stefano and coworkers fused L-DOPA or dopamine with (*R*)-α-lipoic acid, a radical scavenging antioxidant that is taken up in all neuronal cell types.[62, 63] α-Lipoic acid is rapidly reduced intracellularly to dihydrolipoic acid (DHLA), which has been found to lower the redox activity of free iron and copper without extracting the metals from protein sites.[64] The hybrid molecules (one example shown as **16** in **Figure 10**) are enzymatically hydrolyzed in human plasma to release L-DOPA and DHLA as codrugs, with the idea being that sustained release of therapeutic L-DOPA would coincide with release of an antioxidant that can attenuate iron- or copper-mediated oxidative damage.[62]

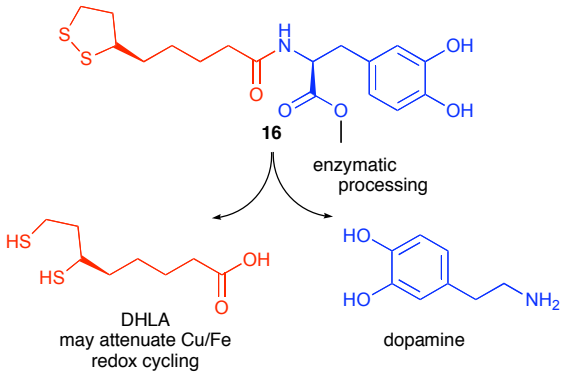

Figure 10: Hybrid molecule 16 fuses L-DOPA with lipoic acid. Enzymatic processing releases DHLA as a metal-attenuating antioxidant and dopamine.[62]

1.4.2 Radical scavaging/ iron binding hybrid molecules

In another hybrid approach, Bebbington *et al.* combined the radical scavaging properties of *tert*-butylphenolic antioxidants with the metal-chelating

hydroxypyridinone unit of deferiprone; an example of one of these hybrid molecules is shown as **17** in **Figure 11**.[65, 66] The dual-action agents were shown to inhibit lipid peroxidation in rat brain homogenates and protect cells against toxicity induced by ROS-generating iodoacetate.[65] Some of the derivatives showed superior neuroprotection compared to dual administration of antioxidants like BHT (butylhydroxytoluene) or Trolox and deferiprone.[65]

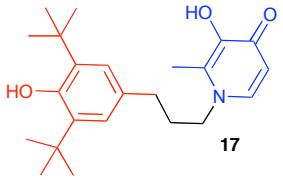

17

Figure 11: Structure of BHT antioxidant (red) fused to hydroxypyridinone chelator (blue).

1.5 Chelators that target Aβ

1.5.1 Amyloid-binding metal chelators

A diagnostic feature of Alzheimer's disease includes the formation of extracellular plaques composed primarily of aggregated amyloid beta peptide (Aβ).[67] Metal ions, particularly $Cu^{+/2+}$ and Zn^{2+} but also $Fe^{2+/3+}$, accelerate Aβ peptide aggregation *in vitro* and have been found at elevated levels in neurotoxic oligomers.[68] The notion that metal chelation could be a promising treatment option for Alzheimer's was encouraged by promising phase IIa clinical trials of clioquinol (**Figure 12**), a derivative of 8-hydroxyquinoline.[69, 70] However, as expressed in the recurrent theme of this review, it is challenging to use general chelating agents to mitigate damaging effects of some metal ions without disturbing the beneficial properties of others. In an attempt to target metal-binding agents directly to amyloid fibrils, several groups have developed

multifunctional agents that combine a metal-chelating unit with an amyloid-binding unit.

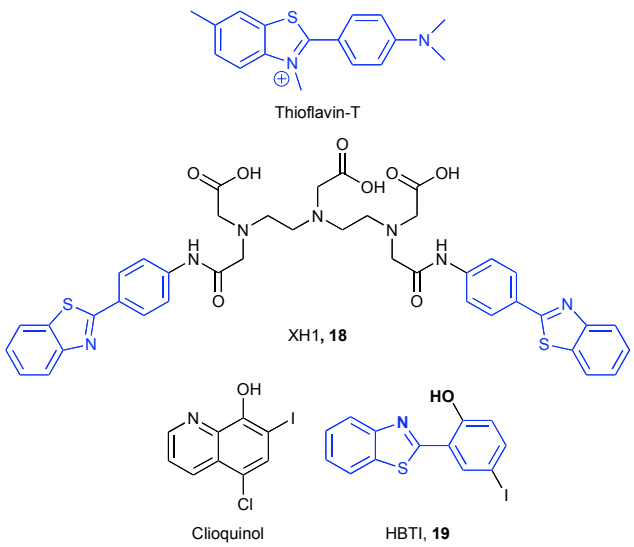

Figure 12: Examples of chelators that incorporate features of thioflavin-T as an amyloid-directing group. XH1 (18) contains an aminocarboxylate binding site, whereas HBTI (19) uses an O/N bidentate unit reminiscent of clioquinol.

Thioflavin-T is a traditional dye used as a marker to detect amyloid deposits in tissue sections because of its strong affinity for amyloid fibrils. Amyloid-targeted chelators have therefore been designed that borrow the core structure of thioflavin-T and modify it with metal-binding functionality. Two examples are shown in **Figure 12**. The bifunctional metal chelator XH1 (**18**), wherein two amyolid-binding units flank an aminocarboxylate chelating unit, was shown to minimize Zn^{2+}-induced $A\beta_{1\text{-}40}$ aggregation *in vitro* and attenuate Aβ amyloid pathology in a transgenic mouse model without toxicity.[71]

In another example, virtual screening methods were employed to find compounds with combined features of thioflavin-T and clioquinol, along with common druglike properties and a lipophilic balance that would enable passage through the BBB.[72] One of the compounds identified is shown in **Figure 12** in its iodinated form

(HBTI**, 19**), which could permit its use as a non-invasive imaging agent.[72] HBTI is comparable to clioquinol in its ability to reduce both Zn^{2+} and Cu^{2+}-induced Aβ aggregation, as confirmed by the Aβ aggregation turbity assay.[72] In addition, fluorescent measurements of HBTI demonstrate significant changes in the presence of amyloid fibrils, indicating that the compound is intercalating within the peptide aggregates as envisioned in the design of the multifunctional agent.[72]

1.5.2 Prochelators activated by Cu–Aβ

In addition to copper's role in accelerating Aβ aggregation, it is also implicated in pro-oxidant mechanisms associated with neuronal damage.[8] In the presence of reductants, Aβ–Cu^{2+} complexes generate H_2O_2 *in vitro*.[73, 74] Excessive H_2O_2 and a surplus of copper ions may therefore create a local environment conducive to oxidative stress. In order to target a chelator for conditions that mimic early Alzheimer's pathology, we adapted our boronate prochelator strategy to create the hydroxyquinoline-based prochelator QBP (**20**).[75] In the absence of H_2O_2, QBP does not prevent or disaggregate metal-promoted Aβ aggregates, a feature that may be beneficial as it may not be desirable to disaggregate already formed plaques. In the presence of ascorbic acid and O_2, however, Cu^{2+}–Aβ assemblies generate enough H_2O_2 to convert QBP to the hydroxyquinoline metal chelator that diminishes copper's ROS-forming reactivity and inhibits further Aβ aggregation (**Figure 13**).[75]

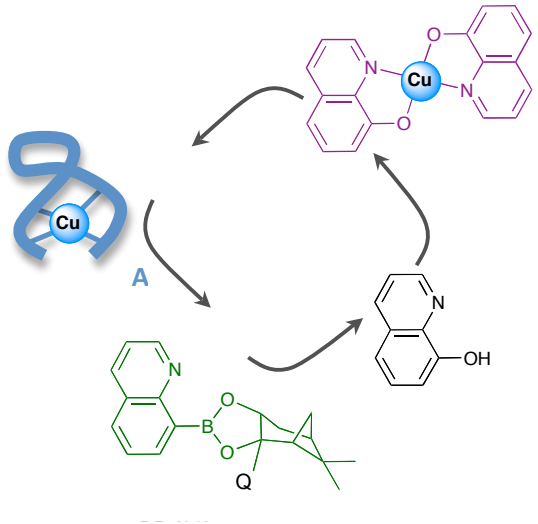

Figure 13: The H_2O_2 generated from Cu-Aβ species in the presence of O_2 and ascorbic acid unmasks prochelator QBP (20) to release 8-hydroxyquinoline that extracts Cu^{2+} from Aβ and prevents further redox-cycling and Aβ aggregation.

1.5.3 Artificial peptidases to break up Aβ peptides

In the aforementioned examples, the overall strategy is to use a chelating agent to extract metals from Aβ in order to prevent aggregation and ROS formation. Suh and coworkers recently introduced a completely different paradigm where a metal complex is used to catalyze the hydrolytic degradation of neurotoxic Aβ oligomers.[76] To develop these artificial Aβ-specific proteases, they screened a library of compounds that combine a Co^{III} cyclen complex as the catalytic center with aromatic moieties having known affinity for Aβ plaques.[76] One of the lead compounds (**21**) that was capable of cleaving Aβ oligomers is shown in **Figure 14**. By altering binding sites, linkers, and catalytic units, protein-cleaving catalysts specific for other proteins have also been developed.[77]

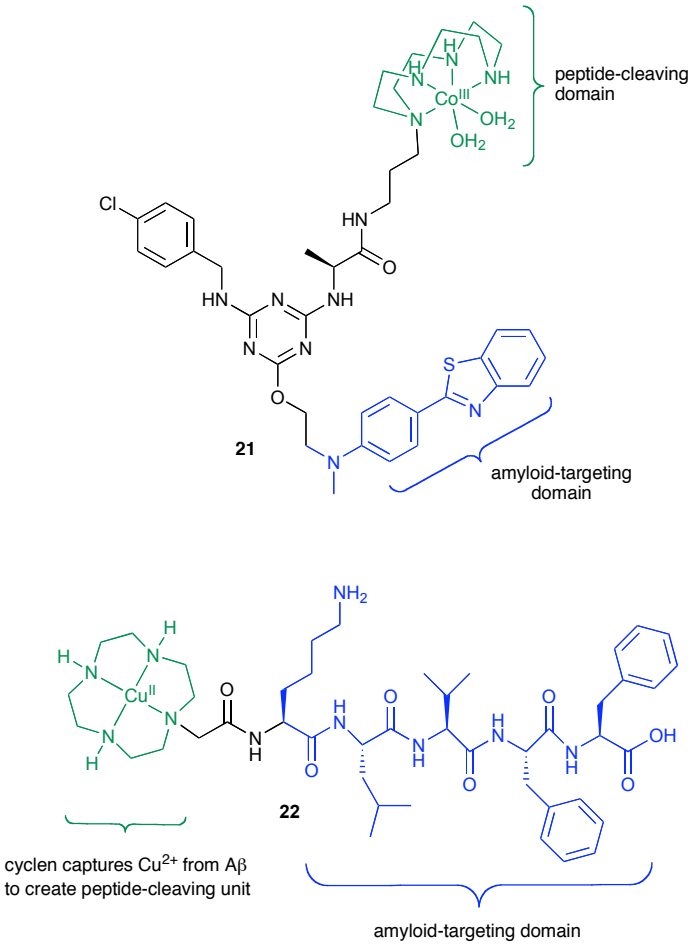

Figure 14: Catalytic Co(III) (21) and Cu(II)-cyclen (22) chelators found to break up Aβ peptides.

In an extension of this protein cleaving tactic, Wu *et al.* reasoned that cyclen would be able to extract copper from Aβ to generate a hydrolytically active complex that could then degrade Aβ.[78] Their constructs contain cyclen covalently fused to an Aβ recognition motif such as the peptide sequence Lys-Leu-Val-Phe-Phe in **22** in **Figure 14**, or curcumin. *In vitro* the cyclen can be metallated by competing with Aβ for Cu(II) to generate the active [Cyc(Cu)-KLVFF] complex that inhibits Aβ oligomerization, suppresses H_2O_2 formation, and produces Aβ peptide cleavage fragments.[78] Furthermore, the apo Cyc-KLVFF hybrid complex was shown to rescue cultured

neurons from Aβ/Cu-induced toxicity, suggesting that it is able to acquire Cu(II) *in situ* to generate the active compound.[78]

1.6 Metal chelators with enzyme inhibitory activity

1.6.1 Monoamine oxidase (MAO) dual action agents

The substantia nigra is a small part of the basal ganglia which is important for movement, reward, and addiction and is the region most affected in Parkinson's disease. In addition to elevated levels of iron in the substantia nigra, the brains of Parkinson's and Alzheimer's patients also show increased activity of monoamine oxidases (MAO), enzymes that oxidatively degrade neurotransmitters like dopamine and generate H_2O_2 as a byproduct.[79] These factors, combined with diminished antioxidant stores of glutathione, lead to a localized environment primed for oxidative stress. In order to increase the effectiveness of iron chelation as a strategy against these diseases, multifunctional agents have been developed that combine iron chelation ability with MAO inhibition.[79, 80]

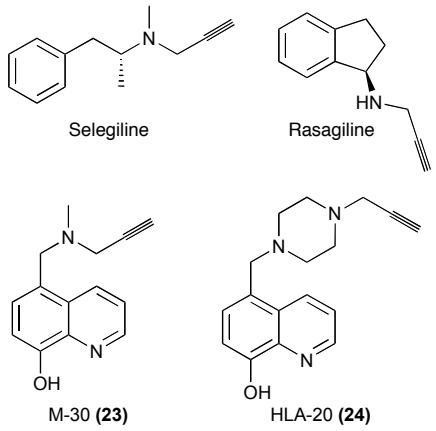

Figure 15: Structures of bifunctional metal-ion chelators, M-30 (23) and HLA-20 (24) that contain an *N*-propargylamine moiety found in MAO inhibitors like Seleginline and Rasagiline.

Both of the lead compounds M-30 (**23**) and HLA-20 (**24**) shown in **Figure 15** contain a brain-permeable 8-hydroxyquinoline chelating unit together with an *N*-

propargylamine moiety. The latter has been found to be responsible for the neuroprotective effects of rasagiline and selegiline, two MAO inhibitors used clinically for treating Parkinson's patients.[81] *In vitro* the bifunctional agents coordinate Fe^{3+} to give 3:1 ligand:metal complexes that inhibit lipid peroxidation at levels comparable to desferrioxamine, while also showing modest MAO inhibitory activity and reasonable cell permeability.[80, 82] The compounds show significant protective effects in cell culture models used for studying neuronal oxidative stress and show a wide range of pharmacological activities that include regulation of the amyloid precursor protein (APP) and reduction of Aβ peptide levels.[82-84] The propargyl substituent on the chelator plays a crucial role in the multifaceted activity of M-30 and HLA-20 that make these compounds promising for future development.[85]

1.6.2 Acetylcholinesterase (AChE) triple action agents

Acetylcholinesterase (AChE) is the enzyme responsible for breaking down acetylcholine, a neurotransmitter that is in short supply in Alzheimer's disease. Classical inhibitors of AChE, like tacrine, the first drug approved for Alzheimer's, block the active site in order to normalize cholinergic levels and improve cognitive function.[86] They do not, however, address the underlying pathology. In addition to its hydrolysis active site, AChE also contains a peripheral anionic site that has been identified as being responsible for promoting Aβ fibrillization. Dual binding site inhibitors that block both the active site and the peripheral anionic site are being sought as they potentially could alleviate cognitive symptoms associated with acetylcholine deficiency while simultaneously reducing Aβ fibrillization, which is believed to be central to the disease mechanism.[86]

In order to take this concept one step further, Bolognesi *et al.* modified a dual-action AChE inhibitor with a metal chelating function to create the triple action agent **25**

shown in **Figure 16**.[87] The parent inhibitor, in which two tacrine units were linked together via a polymethylene spacer, had been validated for its ability to interact with both the catalytic and peripheral sites.[88] By incorporating either carbonyl or oxalamide functional groups into the spacer, the resulting inhibitors also maintain some ability to interact with divalent metal ions. The new bis-tacrine derivatives showed potent AChE inhibition, were able to reverse AChE-induced Aβ fibrillization, and showed spectral changes in the presence of Cu^{2+} or Fe^{2+} indicating metal binding ability.[87] Although the modest μM affinities observed for these divalent metals might not be strong enough to extract metals from Aβ, the potential of generating triple-action AChE inhibitors that incorporate metal chelation was demonstrated.

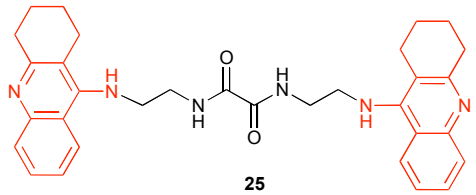

25

Figure 16: A bis-tacrine molecule (25) where the linker can interact with metal ions. The tacrine units are colored in red. 25 has been found to inhibit AChE activity, reverse AChE-induced amyloid fibrillogenesis, and bind metal ions.

Youdim and Fridkin have also recently incorporated AChE inhibition into a multifunctional chelator. In this case, they masked their existing multifunctional chelator HLA-20 (**24**) with an AChE inhibiting moeity to generate a prochelator that requires AChE enzyme activation to release the metal-binding functionality, **Figure 17**.[89] The prochelator **26** is an amalgamation of structural features found in HLA-20 in addition to rivastigmine and donepezil, two AChE inhibitors currently in clinical use. The *N*-benzylpiperidine unit of donepezil targets the peripheral site of AChE, while the carbamyl and ethylmethylamino moieties of rivastigmine bind at the active site. The prochelator **26** inhibited AChE activity with an IC_{50} value of 0.5±0.06 μM that was slightly more potent than rivastigmine.[89] Furthermore, it was found that AChE

efficiently cleaves the carbamyl protecting group to release the quinolinol which forms 2:1 and 3:1 complexes with Cu^{2+} and Fe^{3+}, respectively.[89] Compared with HLA-20, **26** exhibits lower cytotoxicity in SH-SY5Y neuroblastoma cells, further substantiating the prochelator strategy for minimizing toxicity associated with generalized metal chelation.

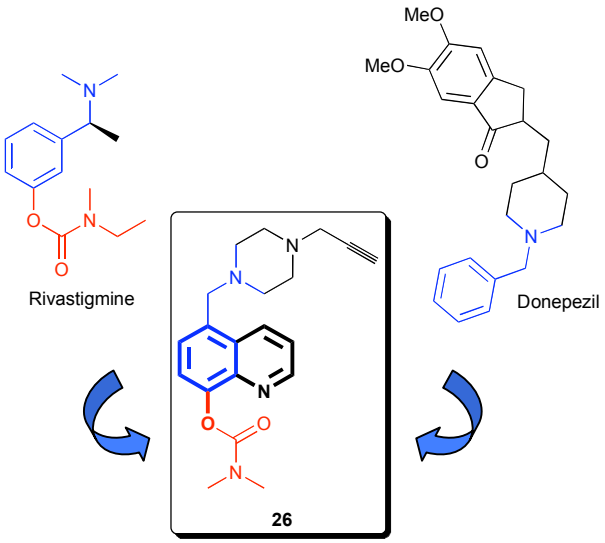

Figure 17: The multifunctional prochelator 26 combines structural features of HLA-20 (24, see Figure 15) and AChE inhibitors rivastigmine and donepezil. The carbamyl group is cleaved by AChE to release the 8-hydroxyquinoline metal binding group (highlighted in bold).

1.7 Conclusions

Metal chelation research aimed at developing potential treatments for neurodegenerative diseases such as Alzheimer's and Parkinson's is moving in a new direction that blends metal chelation with additional functionality. Chapter one has highlightighted some of the creative approaches synthetic and inorganic chemists are taking to generate novel compounds that not only bind metals, but do so in ways that mitigate their potential cellular damage while also providing some element of specificity for disease conditions. These various elements include moieties that target the compounds across the blood-brain barrier or provide a trigger to release the metal-binding agent when the local environment is under conditions of oxidative stress. Other

design strategies are used to create hybrid molecules that combine metal chelation with either antioxidant or enzyme inhibitory moieties, or domains that target the chelator to amyloid fibrils. Many of these compounds are at a very early stage of development, and significant work is still required to test these strategies in cell and animal models of disease. The concepts, however, may have broad applicability in a range of conditions, including cancer and bacterial and viral infection, where interference in cellular metal regulation via targeted metal chelation may provide a therapeutic angle.[90]

2. Prochelator, BSIH, Strategy for Inhibiting Oxidative Stress via Iron Chelation

2.1 Background and Significance

As previously stated, research on iron chelation therapy agents has moved beyond binding metals alone. Researchers have realized that it is necessary to functionalize the chelator to not only bind metals but also to perform other functions, for instance, to prevent oxidative damage from occurring.[50, 51, 91, 92] By making chelators that act selectively on certain tissues, their effects might be enhanced while toxicity is reduced.[93] Our group has designed masked iron chelators that bind iron selectively when activated in the presence of H_2O_2. SIH, salicylaldehyde isonicotinic acid hydrazone, is a well known aroylhydrazone chelator that shows promise for chelation therapy because of favorable attributes of membrane permeability and high affinity iron binding.[21, 50, 93, 94] The masked chelator, BSIH, is modeled after SIH, differing by a boronic pinacol ester masking the phenolic oxygen that is essential to iron binding, **Scheme 2.**

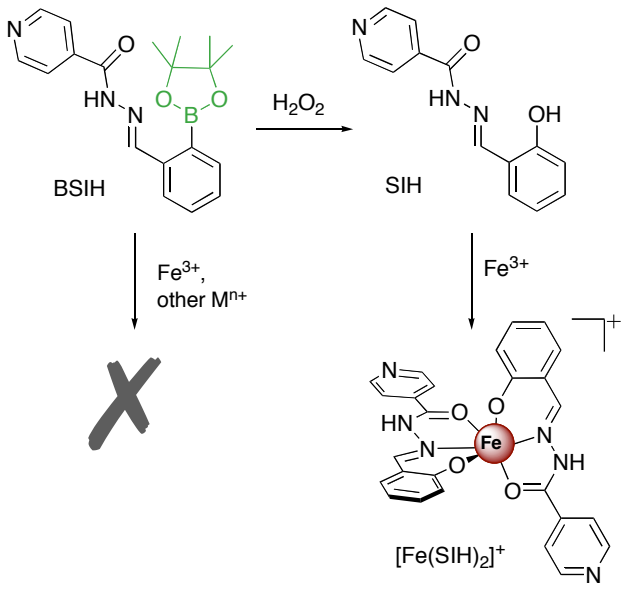

Scheme 2. The masked chelator, BSIH (12), binds Fe^{3+} only following deprotection by H_2O_2.[50]

In its masked form, BSIH has little to no affinity for metal ions. **Scheme 2** shows that the boronic ester on BSIH reacts with hydrogen peroxide to convert BSIH to SIH, thus allowing the chelator to bind iron and prevent hydroxyl radical formation.[50] BSIH itself shows protection against cell death induced by hydrogen peroxide in cultured retinal pigment epthelial cells.[52] Importantly, prolonged and repetitive exposure of healthy cells to BSIH was not toxic, whereas similar treatment with SIH or DFO caused cell death, presumably due to metal depletion.[52] Several analogs of BSIH have been studied to tune properties including lipophilicity, iron binding affinity, and the rate of hydrogen peroxide dependent unmasking of the prochelator.[51] It was found that modifications made to the aroyl ring of the chelators tune their iron affinity, whereas modifications on the boron-containing ring of the pro-chelators attenuate their reaction rates with hydrogen peroxide. Specifically, a methoxy derivative pro-chelator (p-OMe)BASIH was found to react with hydrogen peroxide nearly 5 times faster than the

chloro derivative (m-Cl)BASIH.[51] The rate of oxidation from the pro-chelator to chelator as well as the metal binding affinity of the chelator influenced the overall ability of these molecules to inhibit hydroxyl radical formation catalyzed by iron or copper in the presence of hydrogen peroxide and ascorbic acid. This finding suggests that the pro-chelator strategy may be effective for turning on metal chelation only under oxidative stress conditions.

At this time a set of second-generation pro-chelators and their respective chelators have been synthesized, and are listed in **Table 1**. Compared to the first generation pro-chelator/chelator, BSIH/SIH, changes have been made to the ligands, where the position of the nitrogen on the aroyl ring was changed to the meta (BSNH/SNH) and ortho (BSPH/SPH) position with respect to the hydrazone as compared to BSIH, which has the nitrogen in the para position, **Table 1A**. These modifications have been made to study the effect of the nitrogen's position on the aroyl ring with respect to the affinity of the ligand to the iron. In addition, a pro-chelator was synthesized with a diethanolamine boronic ester mask, replacing the pinacol boronic ester moiety (DEA-BSIH) from BSIH, **Table 1B**. The decision to change the pinacol boronic ester to a diethanolamine ester was made to study changes in the rates of oxidation to the chelator form. A pro-chelator and its respective chelator have also been synthesized with modifications to the ring containing the B- or OH- (FMDOP-Bpin-IH/ FMDOP-IH) to examine changes in iron affinity and/or the rate of oxidation of the boronic ester with H_2O_2, **Table 1C**. In order to increase the stability of the well-known chelator, SIH, a derivative chelator was synthesized with a methyl group on the imine carbon of SIH (HAP-INH), **Table 1D**. The solubility of the pro-chelators and chelators has been determined in de-ionized water, 20 mM sodium phosphate buffer at pH 7.4, 92% MEM: 8% DMSO, MEM, and 100 mM NaOH. The stability of the pro-chelators/

chelators has been examined in MEM at pH 7.4 and 100 mM NaOH, for solubility purposes. Kinetics of activation of the pro-chelators DEA-BSIH and BSIH have been examined in H_2O_2 and tertbutyl-hydroperoxide (for BSIH only). The apparent stability constants of the chelators with iron at pH 7.4 were also determined.

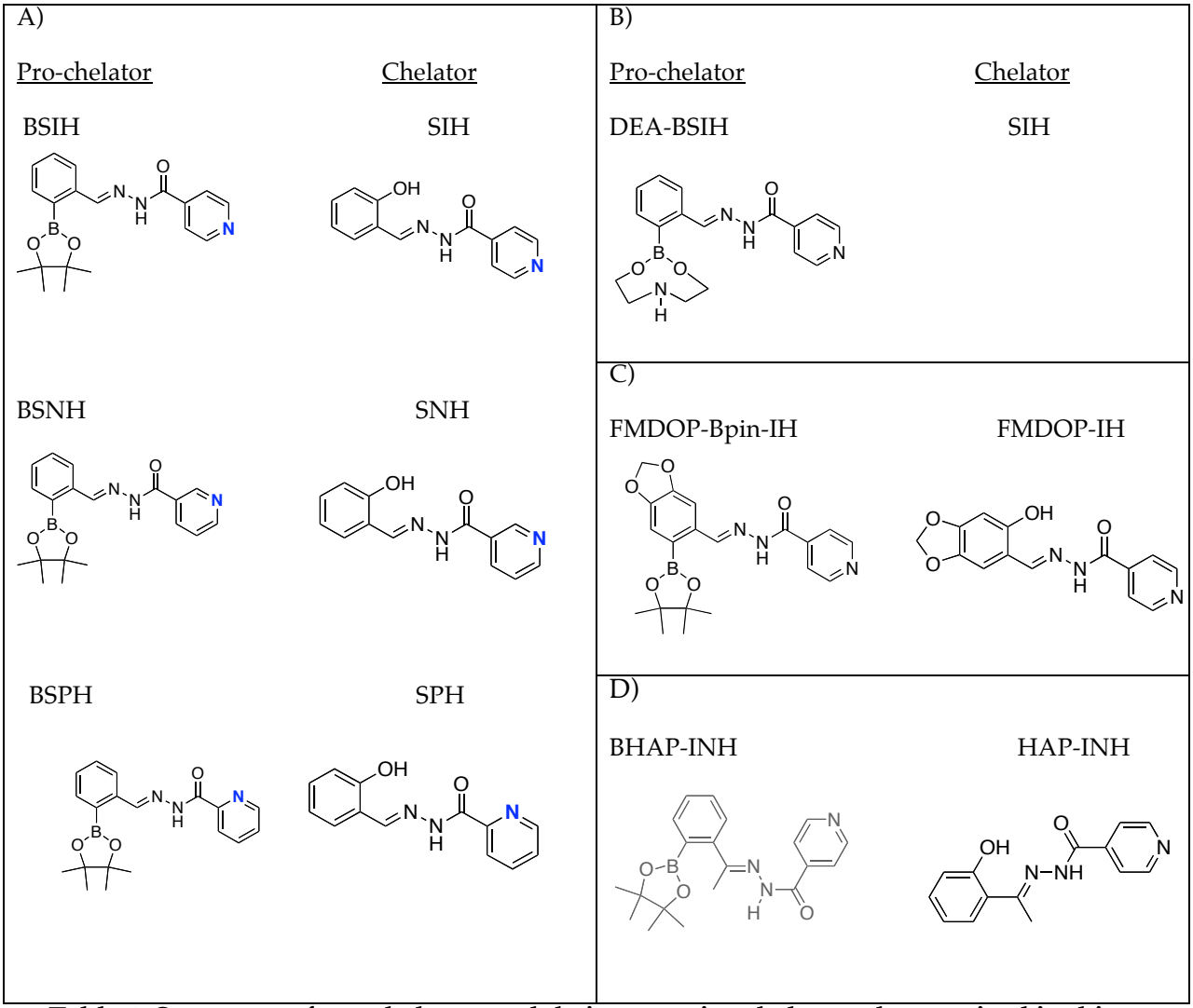

Table 1. Structures of pro-chelators and their respective chelators characterized in this document. A) The position of the nitrogen on the aroyl ring was changed to tune iron binding, B) DEA was used in place of pinacol to tune the rate of oxidation, C) Modifications to the boron containing ring were made to tune iron binding and oxidation rate, D) Derivative of SIH with a methyl next to the imine carbon shown to increase stability of the chelator.

2.2 Experimental Section

2.2.1 Materials and Methods

Chemicals were obtained from Sigma-Aldrich or Acros Organics without further purification unless otherwise noted. The 2-formylphenylboronic acid and the 2-formylphenylboronic acid pinacol ester were purchased from Combi-Blocks, Inc.; 2-picolinyl hydrazide was purchased from ABCR GmbH and Co.; Aqueous solvents were prepared from nanopure water and all organic solvents were reagent grade. ^{1}H-NMR spectra were recorded on a Inova 400 spectrometer; δ values are in ppm. Mass spectra (ESI-MS) were measured on an Agilent 1100 Series LC/MSD trap spectrometer with a Daly conversion dynode detector. UV-vis spectra were recorded on a Varian Cary 50 Conc spectrophotometer.

2.2.2 Synthesis

2.2.2.1 Synthesis of Pro-chelators

BSIH: (E)-N'-(2-(4,4,5,5-tetramethyl-1,3,2-dioxaborolan-2-yl) benzylidene) isonicotinohydrazide: BSIH was prepared as described previously.[50] Insonicotinic acid (1 mmol, 0.137 g) was dissolved in pH 4.5 0.1 M sodium acetate buffer and added to a round bottom flask equipped with a stirring bar. The 2- formylphenyl boronic acid (1 mmol, 0.232 g) was added dropwise to the solution. The reaction mixture was stirred at 100 °C for 5 min and then cooled in an ice bath. The beige solid was collected via vaccum filtration and was rinsed with water and ether (0.220g, 63% yield). 1H NMR (DMSO): δ 1.342 (12H), 7.45 (2H), 7.57 (1H), 7.67 (1H), 7.74 (2H), 8.03 (1H), 8.78 (2H), 8.96 (1H), 12.18 (1H, s) ESI-MS: m/z 352.1 $(M + H)^{+}$.

BASIH: 2-formylphenylboronic acid (1 mmol, 0.150 g), dissolved in minimal MeOH, and isonicotinic acid hydrazide (1 mmol, 0.137 g), in pH 4.5 0.1 M sodium acetate buffer, were added to a round bottom flask equipped with stirring bar. The

reaction mixture was stirred in the flask for 6 minutes at 100 °C and then cooled in an ice bath. A white product precipitated out of solution and was filtered with DI-water and collected *via* vacuum filtration (0.495 g, 92% yield). ^{1}H-NMR (CD_3OD 400 MHz): δ 8.75 (2H), 8.46 (1H), 7.88 (2H), 7.66 (1H), 7.44 (2H), 7.39 (1H); ESI-MS: m/z 270.0 $(M + H)^+$.

DEA-BSIH: (E)-N'-(2-(1,3,6,2-dioxazaborocan-2 yl) benzylidene)isonicotino-hydrazide: BASIH (1mmol, 0.2692 g) and diethanolamine, DEA, (1.2 mmol, 0.1262 g) were dissolved in minimal DMF and combined in a round bottom flask. The reaction was stirred for 20 min at room temperature. The white precipitate was collected by vacuum filtration, washed with cold DMF and dried *in vacuo* to yield a white precipitate. (0.200 g, 59.2% yield) ^{1}H-NMR (D_2O 400 MHz): δ 8.61 (2H), 7.714 (1H), 7.52 (1H), 7.49 (2H), 7.43 (1H), 7.41 (1H), 7.38 (1H), 3.84 (4H), 3.17 (4H). ESI-MS: m/z 339.1 $(M + H)^+$.

BSNH:(E)-N-(2-(4,4,5,5-tetramethyl-1,3,2-dioxaborolan-2-yl)benzylidene nicotinohydrazide: The 2-formylphenyl boronic acid pinacol ester (1 mmol, 0.2328 g) was added to a nearly saturated solution of nicotinic acid (1 mmol, 0.1378 g) in pH 4.5 0.1 M sodium acetate buffer. The reaction was stirred for 12 min at 100 °C and then cooled in an ice bath. The beige solid precipitate was collected by vacuum filtration. (0.195 g, 55%) ^{1}H-NMR (d_6-DMSO 400MHz): δ 12.148 (1H), 9.057 (1H), 8.947 (1H), 8.778 (1H), 8.258 (1H), 8.040 (1H), 7.743 (1H), 7.564 (2H), 7.442 (1H), 1.343 (12H). ESI-MS: m/z 352.1 $(M + H)^+$.

BSPH: (E)-N-(2-(4,4,5,5-tetramethyl-1,3,2-diocaborolan-2-yl) benzylidene) picolinohydrazide: A similar procedure to the one above was performed except the nicotinic acid was replaced by 2-picolinyl hydrazide and the reaction was stirred for 10 min at 100 °C. A beige solid was collected at 53% yield. (0.186 g). ^{1}H-NMR(d_6-DMSO400MHz): δ 12.239 (1H), 9.014 (1H), 8.121 (1H), 8.061 (1H), 8.004 (1H), 7.694 (2H), 7.553 (1H), 7.432 (1H), 1.346 (12H). ESI-MS: m/z 352.1 $(M + H)^+$.

BAHAP-INH: (1-Hydroxy-4-methyl-1H-benzo[*d*][1,2,3]diazaborinin-2-yl)-pyridin-4-yl-methanone: Isonicotinic acid (2 mmol, 0.328 g) and 2-acetylphenylboronic acid (2 mmol, 0.274 g) in ethanol were added to a round bottom flask equipped with a stirring bar followed by a few drops of glacial acetic acid. The reaction mixture was heated for 6 minutes at 100 °C and was then cooled to room temperature. The white solid product was rinsed with ethanol and filtered *via* vacuum filtration. (0.431 g, 81% yield). ^{1}H-NMR(d_6-DMSO 400MHz): δ 8.73 (2H), 7.78 (2H), 7.67 (2H), 7.56 (2H); ESI-MS: m/z 266.0 $(M + H)^+$

FMDOP-Bpin ester-IH: (E)-N-((5-(4,4,5,5-tetramethyl-1,3,2-diozaborolan-2yl)benzoic[d][1,3]dioxol-6-yl)methylene)isonicotinohydrazide: 2-formyl-4,5-methylenedioxyphenylboronic acid (1 mmol, 0.1942 g) was diluted in minimal methanol and the isonicotinic acid hydrazide (1 mmol, 0.1378 g) was dissolved in pH 4.5 0.1 M sodium acetate buffer. The reactants were combined in a round bottom flask and stirred for 6 min at 100 °C. The solid white boronic acid hydrazone (FMDOP-BAH) was cooled in ice and collected by vacuum filtration. (0.274 g, 88%). ^{1}H-NMR (CD_3OD 400 MHz): δ 8.752 (2H), 8.391 (1H), 7.875 (2H), 7.736 (1H), 6.859 (2H)

A portion of the FMDOP-BAH (0.24 mmol, 0.078 g) and pinacol (0.3 mmol, 0.0334 g) were then dissolved in DMF and added to a round bottom flask. The reaction stirred for 21 h at room temperature and was then collected by vacuum filtration. The filtrate was collected and dried in vacuo. (0.076 g, 82%) ^{1}H-NMR (DMSO 400 MHz): δ 12.150 (1H), 8.956 (1 H), 8.785 (2 H), 7.807 (2 H), 7.523 (1 H), 7.134 (1 H), 6.119 (2 H) 1.325 (12 H) ESI-MS: m/z 396.1 $(M + H)^+$

2.2.2.2 Synthesis of Chelators

SIH: (E)-N'-(2-hydroxybenzylidene)isonicotinohydrazide: SIH was prepared as described previously by a Schiff-base condensation.[50, 91, 94, 95] The isonicotinic acid

hydrazide (1 mmol, 0.137 g) was dissolved in 0.1 M pH 4.5 sodium acetate buffer and stirred at 100 °C over an oil bath. The salicylaldehyde (1 mmol, 0.122 g), a clear oil, was immediately added dropwise to the round bottom flask and the reaction mixture stirred for 5 min 100 °C. The white product precipitated out of solution and was collected via vacuum filtration and washed with water. H NMR (DMSO): δ 6.933 (2H, m), 7.319 (1H, td, J = 1.68, J = 6.69), 7.608 (1H, dd, J = 1.49, J = 7.67), 7.846 (2H, dd, J = 1.65, J = 4.4), 8.682(1H, s), 8.802 (2 H, dd, J = 1.59 , J = 4.4), 11.075 (1H, s), 12.298 (1H, s). MS (ESI): m/z 242.1 ($M + H^+$), 264.1 ($M + Na^+$), 240.1 ($M - H^+$).UV-vis (1:1 MeOH: 20 mM sodium phosphate buffer) nm (M^{-1} cm^{-1}): 214 (16,839), 286 (16,455), 332 (13,934).

SNH: (E)-N-(2-hydroxybenzylidene)nicotinohydrazide: Both the salicylaldehyde (2 mmol, 0.2442 g) and the nicotinic hydrazide (2 mmol, 0.2762 g) were dissolved in pH 4.5 0.1 M sodium acetate buffer and combined in a round bottom flask. The reaction was stirred for 8 min at 95°C and then cooled over ice. The white solid was collected by vacuum filtration. (0.506 g, 105%). (Further purification is necessary) ^{1}H-NMR (d_6-DMSO 400 MHz): δ 12.245 (1H), 11.139 (1H), 9.909 (1H), 8.785 (1H), 8.652 (1H), 8.288 (1H), 7.603 (2H), 7.316 (1H), 6.933 (2H). ESI-MS: m/z 242.1. $(M + H)^+$; UV-vis (1:1 MeOH: 20 mM sodium phosphate buffer) nm (M^{-1} cm^{-1}): 214 (16,267), 286 (18,660), 332 (12,985).

SPH: (E)-N-(2-hydroxybenzylidene)picolinohydrazide: A simlar procedure to the one above was performed except the nicotinic hydrazide was replaced by 2-picolinyl hydrazide and the reaction was stirred for 10 min. A white solid was collected (0.432 g, 90%). ^{1}H-NMR (d_6-DMSO 400 MHz): δ 12.506 (1H), 11.418 (1H), 8.839 (1H), 8.741 (1H), 8.150 (1H), 8.073 (1H), 7.690 (1H), 7.484 (1H), 7.316 (1H), 6.933 (2H). ESI-MS: m/z 242.1 $(M + H)^+$; UV-vis (1:1 MeOH: 20 mM sodium phosphate buffer) nm (M^{-1} cm^{-1}): 214 (21,395), 286 (19,197), 332 (18,204).

FMDOP-IH:(E)-N-((5-hydroxybenzoi[d][1,3]dioxol-6-yl)methylene) isocotinohydrazide: A portion of FMDOP-BAH (0.5 mmol, 0.1630 g) was added to 15 mL methanol in a round bottom flask. Hydrogen peroxide (50%) (11 mmol, 623 uL) was added dropwise and the reaction mixture stirred for 2 h. (0.109 g, 77%) ^{1}H-NMR (CD_3OD 400 MHz): δ 8.753 (2H), 8.462 (2H), 7.889 (2H), 6.971 (1H), 6.476 (1H), 5.951 (2H). ESI-MS: m/z 286.1 $(M + H)^+$. UV-vis (1:1 MeOH: 20 mM sodium phosphate buffer) nm (M^{-1} cm^{-1}): 214 (20,476), 263 (15,312), 363 (20,534).

HAP-INH: (E)-N'-(1-(2-hydroxyphenyl)ethylidene)isonicotinohydrazide: HAP-INH was prepared in a similar way that has been described previously.[96] The 2-hydroxyacetophenone (1 mmol, 0.1362 g) was dissolved in ethanol and the isonictotinic acid hydrazide was dissolved in ethanol and catalytic amounts of glacial acetic acid. The reaction was stirred at 90 °C for 19h and monitored by TLC (6:4 hexanes: ethyl acetate). The reaction mixture was then cooled in an ice bath and the white powder was filtered and rinsed with cold ethanol. (0.177 g, 69%) NMR (CD_3OD 400 MHz): δ 8.762 (2 H), 7.908 (2 H), 7.664 (1H), 7.318 (1H), 6.954 (2). ESI-MS: m/z 256 $(M + H)^+$;UV-vis (1:1 MeOH: 20 mM sodium phosphate buffer) nm (M^{-1} cm^{-1}): 214 (26,364), 286 (14,425), 332 (10,962).

2.2.2.3 Synthesis of bis-Iron Complexes

$[Fe(SIH)_2](NO_3)$: $[Fe(SIH)_2]^+$ was synthesized using a procedure previously described.[50, 97] SIH (1.72 mmol, 0.4150 g) was dissolved in 125 mL of MeOH and added to a round bottom flask equipped with stirring bar and refluxed. $Fe(NO_3)_3 \bullet 9H_2O$ was dissolved in 30 mL of MeOH and added dropwise into the refluxing solution. After 1 hour of refluxing at 90 °C, the solution was cooled and the black precipitate was collected via vacuum filtration, washed with ethanol and diethyl ether. MS (ESI): *m/z*

533.9 (M – 2H+), 536.1 (M + H+). In revisiting the $[Fe(SIH)_2]^+$ complex, the extinction coefficient values were adjusted to the following: UV-vis (1:1 MeOH: 20 mM sodium phosphate buffer) nm (M^{-1} cm^{-1}): 294 (31,859), 332 (21,679), 450 (5428.1).

$[Fe(SNH)_2](NO_3)$: $[Fe(SNH)_2]^+$ was synthesized using the same procedure used for $[Fe(SIH)_2]^+$. MS (ESI): *m*/*z* 533.9 (M – 2H+), 536.1 (M + H+). UV-vis (1:1 MeOH: 20 mM sodium phosphate buffer) nm (M^{-1} cm^{-1}): 450 (4952.2)

$[Fe(SPH)_2](NO_3)$: $[Fe(SPH)_2]^+$ was synthesized using the same procedure used for $[Fe(SIH)_2]^+$. MS (ESI): *m*/*z* 534.0 (M – 2H+), 536.2 (M + H+). UV-vis (1:1 MeOH: 20 mM sodium phosphate buffer) nm (M^{-1} cm^{-1}): 450 (4689.4)

$[Fe(FMDOP\text{-}IH)_2](NO_3)$: $[Fe(FMDOP\text{-}IH)_2]^+$ was synthesized using the same procedure used for $[Fe(SIH)_2]^+$. MS (ESI): *m*/*z* 624.2 (M + H^+), 622.0 (M - $2H^+$).

$[Fe(HAP\text{-}INH)_2](NO_3)$: $[Fe(HAP\text{-}INH)_2]^+$ was synthesized using the same procedure used for $[Fe(SIH)_2]^+$. MS (ESI): *m*/*z* 564.2 (M + H^+), 562.0 (M - $2H^+$).

2.3 Results

The solubility and stability of the pro-chelators and chelators were analyzed in various solvents. The oxidation of BSIH and DEA-BSIH to SIH has been evaluated in H_2O_2 and tertbutyl-hydroperoxide (for BSIH only). The conditional stability constants of the chelators with iron have also been evaluated at pH 7.4.

2.3.1 Solubility of pro-chelators/chelators in various solutions

The solubility of the pro-chelators/chelators was analyzed in either de-ionized water, 20 mM sodium phosphate buffer at pH 7.4, 92% MEM: 8% DMSO, MEM, or 100 mM NaOH. To determine solubility, small aliquots of solvent were added to the solid pro-chelator and the solution was placed in the ultrasonic bath. Solubility of the

solutions was monitored by holding the vial to the light and visually observing the solution for any signs of precipitation. Results can be found in **Table 2**.

Table 2. Solubility of the A) pro-chelators and B) chelators in various solutions.

A) Prochelators	DI-H_2O (mM)	MEM (mM)	$NaHPO_4$ pH 7.4 (mM)	8% DMSO (μM)	100 mM NaOH	MEM*
BSIH	177	200	200	50	All Soluble at 1 mM	All soluble at 50 μM
BSNH	118	-	200	50		
BSPH	NS	NS	NS	50		
FMDOP-Bpin-IH	NS	NS	NS	50		
DEA-BSIH	10 mM	-	2 mM			

B) Chelators	DI-H_2O	MEM	92% MEM 8% DMSO (mM)	100 mM NaOH	MEM*
SIH	NS	NS	50	All Soluble at 1 mM	All soluble at 50 μM
SNH	NS	NS	50		
SPH	NS	NS	50		
FMDOP-IH	NS	NS	50		
HAP-INH	NS	NS			

NS = Solubility of the prochelators/chelators were tested at 200 or 500 μM and were not soluble at these concentrations. Solublity below those concentrations is unknown.
MEM*= The pro-chelators/chelators were dissolved in100 mM NaOH and diluted in MEM. The pH was then adjusted to 7.4

2.3.2 DEA-BSIH stability studies by ^{1}H-NMR

Solutions of 10 mM DEA-BSIH were made in water, methanol and 20 mM sodium phosphate buffer at pH 7.4. After 3 h in solution, half of each sample (2.5 mL) was separated and the solvent was removed *in vacuo*. ^{1}H-NMR spectra were collected for each of the 3 samples and analyzed in CD_3OD. After 45 h in solution the remaining solvent was evaporated from each sample and another set of ^{1}H-NMR spectra was collected. Spectrum in **Figure 18A** is standard DEA. **Figure 18B** shows the peaks corresponding to the DEA ester bound on the pro-chelator and **Figure 18C** shows the spectra of DEA-BSIH after being in solution for 45 h in 20 mM sodium phosphate buffer at pH 7.4.

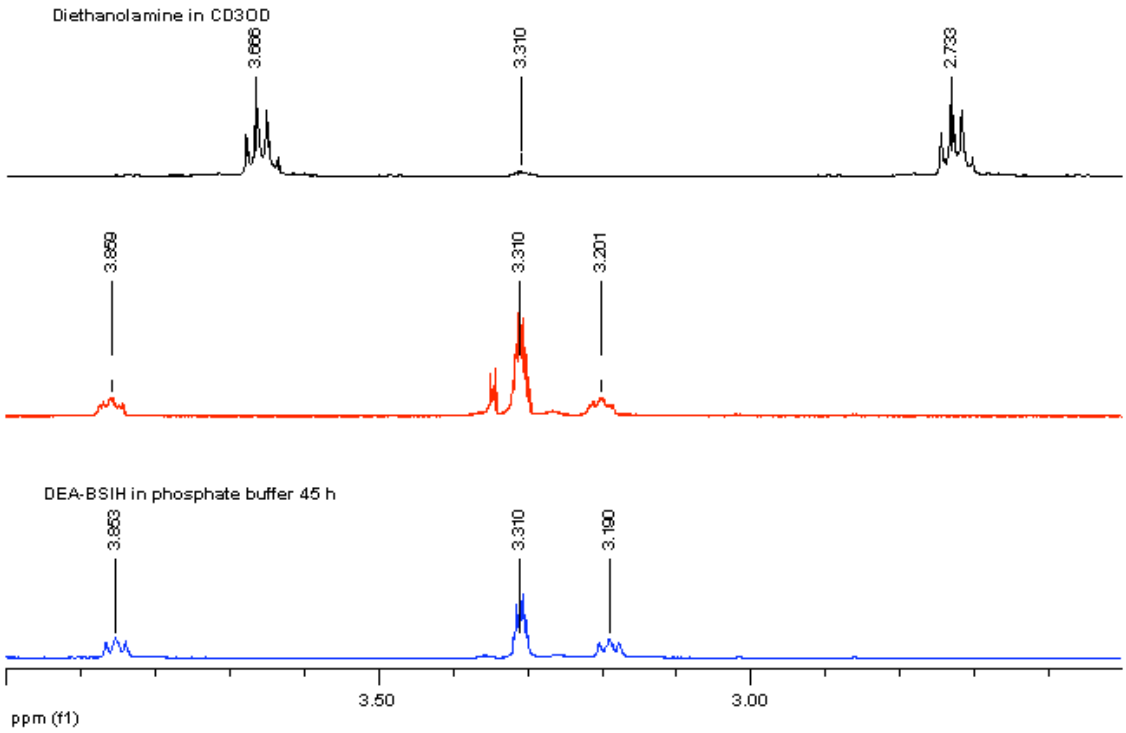

Figure18: ^{1}H-NMR spectra of (a) DEA, (b) DEA-BSIH in 20 mM $NaHPO_4$ buffer at pH 7.4 after 3 h (c) DEA-BSIH in 20 mM $NaHPO_4$ buffer at pH 7.4 after 45 h

2.3.3 Determination of unknown contaminant in BSIH spectra

It was noticed that upon using the same reaction parameters on a continuous basis for the synthesis of BSIH, a peak at 8.5 ppm appeared at different intensities using ^{1}H-NMR, **Figure 19A**. A simple ^{1}H-NMR experiment was performed where the spectrum of BSIH in d_6-DMSO was collected. Immediately following, a couple of drops of D_2O were added to the sample and a second spectrum was collected, **Figure 19B**. It is clear that upon the addition of the D_2O the peak at 8.5 ppm disappears. This finding confirms our hypothesis that the impurity is actually a proton from the hydroxyl group of the boronate species of BSIH.

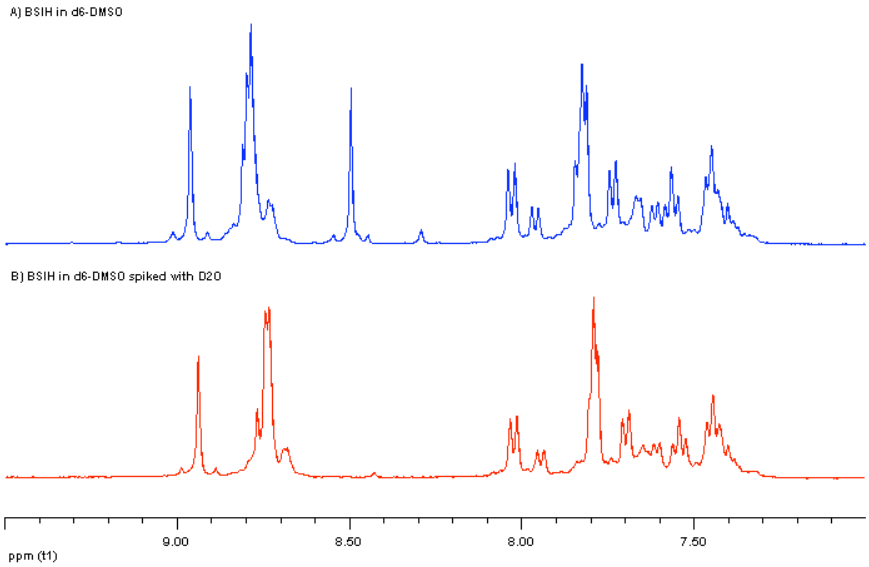

Figure 19. ^{1}H-NMR of BSIH. A) BSIH in d_6-DMSO. B) Immediately following collection of spectra A, the sample was spiked with D_2O and a second set of spectra were collected. The peak at 8.5 ppm clearly disappears in the presence of D_2O indicating the boronate species of BSIH.

2.3.4 Determination of stability in 100 mM NaOH, conditions needed for solubility purposes

The stability of the compounds were examined in 100 mM NaOH solution to determine if the pro-chelators/chelators can be stored in this solution for at least 2 days if frozen without hydrolyzing into their hydrazide and aldehyde/ketone counterparts. Solutions of 1 mM pro-chelators/chelators were made in 100 mM NaOH. The solutions were diluted to 50 μM pro-chelator/chelator and UV-vis spectra were collected after 15 min in solution. After being frozen for 48 h and defrosted for 4 h, another set of spectra was collected. The spectra for DEA-BSIH and FMDOP-Bpin-IH can be seen below, **Figure 20**. While DEA-BSIH showed no changes in it's UV spectra, FMDOP-Bpin-IH showed some changes. The results obtained for the chelators and remaining pro-chelators can be seen in Appendix A.

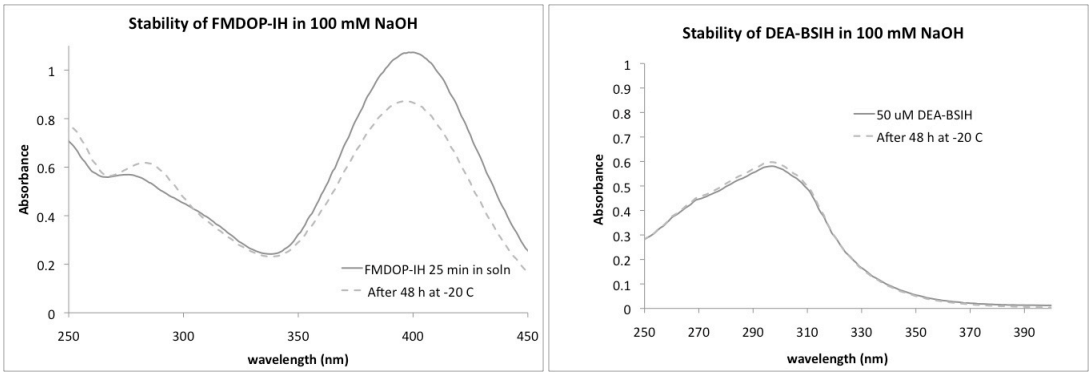

Figure 20: UV-vis spectra of 50 μM solutions of FMDOP-Bpin-IH and DEA-BSIH in 100 mM NaOH before and after freezing at -20 C. The spectra of the other pro-chelators/chelators examined can be found in Appendix A.

2.3.5 Determination of stability in minimal essential media, MEM, conditions for future cell studies

Solutions of 1 mM pro-chelators/chelators were made in 100 mM NaOH. The compounds were diluted to 50 μM with MEM. The pH was adjusted to pH 7.4 with 0.1 mM HCl. Stability of the pro-chelators in MEM at pH 7.4 and 37 °C was analyzed at 0 min, 30 min, 1 h, 2 h, 3 h, 4 h, 21 h using a UV-vis spectrophotometer. **Figure 21** shows the data at 0 min (1.5 h at room temperature), 4 h, and 24 h for DEA-BSIH and SIH. Minimal changes were observed in the spectra for DEA-BSIH where it's respective chelator, SIH, showed significant change. The change seen in the spectra of SIH in cell culture media is consistent with the literature.[52] The spectra for the other pro-chelators and chelators analyzed can be found in Appendix A.

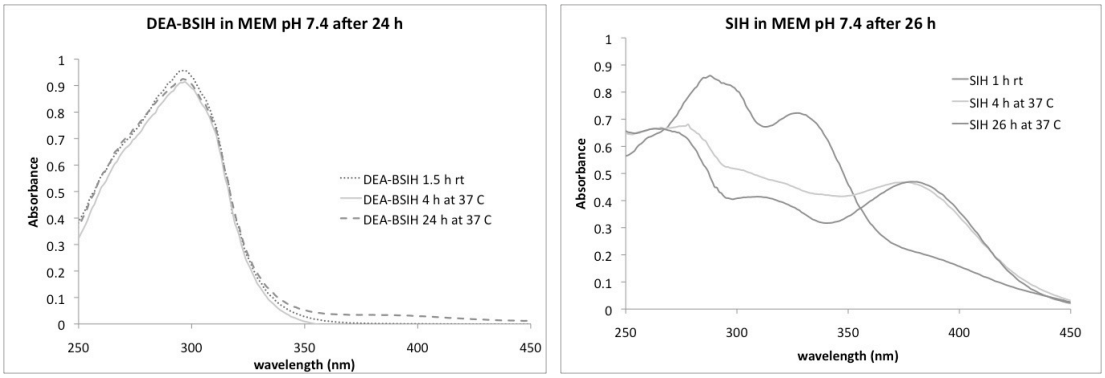

Figure 21: 50 μM solutions of the pro-chelator, DEA-BSIH, and it's respective chelator, SIH, in MEM at pH 7.4 and 37 °C. The spectra of the other pro-chelators/chelators examined can be found in the supplementary section.

2.3.6 Kinetics of Oxidation of Pro-Chelators to Chelators

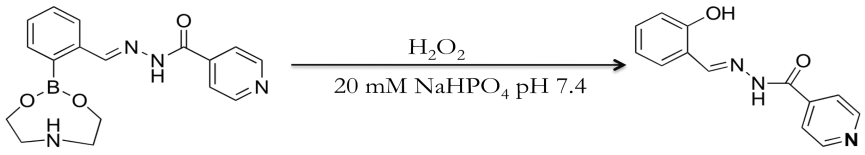

Figure 22. The oxidation of DEA-BSIH to SIH using H_2O_2 in 20 mM $NaHPO_4$ at pH 7.4.

Rate studies of oxidation of BSIH and DEA-BSIH to SIH were performed using pseudo first-order conditions with excess H_2O_2, **Figure 22**. In general, the pro-chelators were dissolved in 50 mM NaOH and then further diluted in the 20 mM sodium phosphate buffer at pH 7.4. Three milliliters of 50 μM BSIH or DEA-BSIH in 20 mM sodium phosphate buffer at pH 7.4 was loaded into a quartz cuvette. Spectra were collected before and after the addition of hydrogen peroxide (0 mM, 0.5 mM, 1 mM, 3 mM, and 5 mM) to the samples. At least 30 scans were collected throughout the kinetic run. The observed pseudo- first order rate constant, k_{obs} (s^{-1}), was determined by plotting the negative slope of the linear fit of a corrected value of the ln (Abs), **Equation 1**, at 380 nm vs time:

$$\ln\left(\frac{Abs_x - Abs_f}{Abs_i - Abs_f}\right) \qquad \text{[Eq 1]}$$

where Abs_x is the absorbance of the time point being analyzed, Abs_f is the absorbance of 50 μM SIH at 380 nm, and Abs_i is the initial absorbance of the reaction mixture before the oxidant is added. The second order rate constant, k ($M^{-1} s^{-1}$), was then determined by plotting the linear fit of k_{obs} (s^{-1}) vs [H_2O_2]. **Figure 23** displays the spectra corresponding to the oxidation of pro-chelator, DEA-BSIH, to its corresponding chelator, SIH, in the presence of 5 mM H_2O_2. The increasing peak at 380 nm corresponds to a spectral feature of SIH.

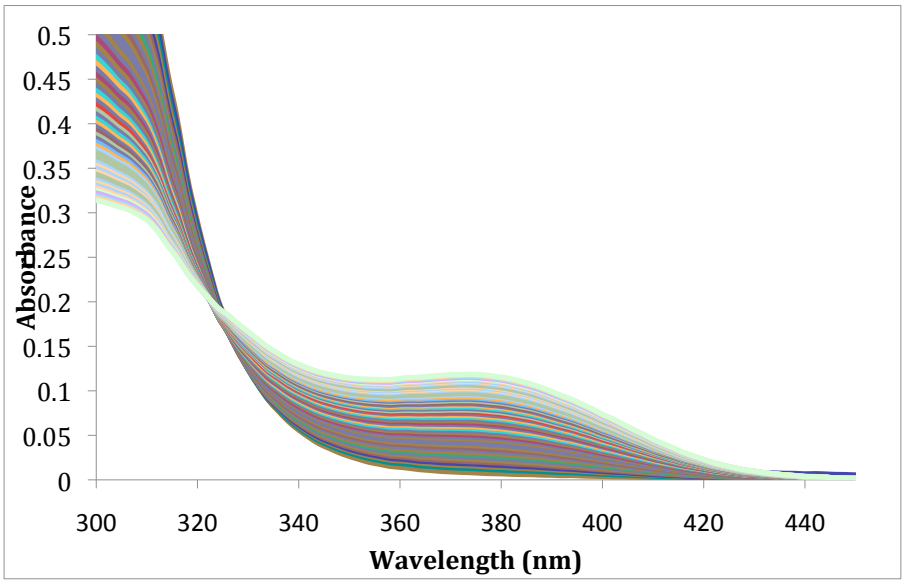

Figure 23. The oxidation of pro-chelator, DEA-BSIH, to its corresponding chelator, SIH, in the presence of 5 mM H_2O_2. The conversion was evaluated in 20 mM sodium phosphate buffer at ph 7.4.

Figure 24 shows a plot of k_{obs} for DEA-BSIH versus concentration of H_2O_2, where the slope of the line equals the second order rate constant for the pro-chelator. The second order rate constant, k, of BSIH at 300 nm was previously determined to be 0.053 $M^{-1} s^{-1}$.[51] Using the corrected value for the ln of absorbance at 380 nm, k= 0.032 $M^{-1} s^{-1}$ for BSIH and k=0.023 $M^{-1} s^{-1}$ for DEA-BSIH. Tert-butyl hydroperoxide was also used as an

oxidant to determine the rate of unmasking of BSIH, however, no reaction was observed.

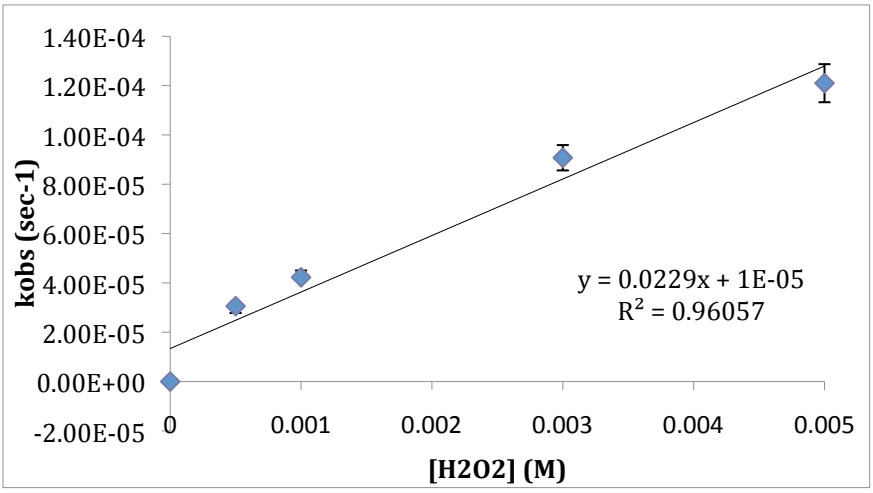

Figure 24. The second order rate constant for DEA-BSIH being oxidized to SIH, Figure 22. The graph shows the plot of k_{obs} vs H_2O_2 concentration for the oxidation of 50 μM BSIH to SIH in 20 mM $NaHPO_4$ buffer at pH 7.4.

2.3.7 Iron binding stability of the chelators

2.3.7.1 Standardization of the iron perchlorate solution

Prior to beginning iron binding studies, the iron (III) perchlorate ($Fe(III)HClO_4$) solution was standardized using procedures previously described.[98] $Fe(III)HClO_4$ (0.10 mol, 17.71 g) and perchloric acid (0.10 mol, 5.023 g) were diluted in dionized water. A UV-vis spectrophotometer was used to detect the absorbance of the iron(III)perchlorate at 260 nm with increasing amounts of solution ranging from 10 µL to 80 µL, keeping the concentration of perchloric acid in excess.

2.3.7.2 Determination of Apparent Stability Constant for Complex Formation with Iron

A competition study with EDTA, ethylenediaminetetraacetic acid, was performed to determine the apparent stability constants for the chelators at pH 7.4. The concentration of EDTA varied from 0.3- 3 mM while the iron(III)perchlorate and the

chelators were held constant at 0.15 mM and 0.45 mM, respectively. The working solution was a 50:50 MeOH: 10 mM HEPES/100 mM NaCl mixture. Each of the solutions was allowed to equilibrate for at least 15 h before spectra were collected. In general, 3 mL of the solutions were loaded into a quartz cuvette and were scanned from 200 nm – 800 nm. A three fold excess of ligand compared to the amount of iron(III) was added to each reaction mixture to ensure a 2:1 binding of chelator to metal. Assuming 2:1 binding of metal to chelator, equations 2-13 were used to determine the apparent stability constant of the complexes.

The overall equilibrium reaction for the SIH/EDTA competition for Fe (III) can be seen in Equation 2. Equations 3 and 5 depict the individual reactions occurring *in situ*. The formation constants of these individual reactions can be seen in equations 4 and 6. The exchange of iron(III) between EDTA and the chelator being studied can be defined by an exchange constant, K_{ex}. An apparent K_{ex}, also written as K'_{ex}, at pH 7.4 was determined experimentally and is defined in equation 7. In this document a prime is used after the K to indicate the pH is held constant at 7.4. K'_{ex} can also be expressed as **Equation 8** where $K'_{Fe(SIH)2}$ is equal to $K_{Fe(SIH)2}$ at pH 7.4, **Equation 9**. The value of $K'_{Fe\text{-}EDTA}$ is defined in **Equation 10**. The β value of EDTA at pH 7.4, $10^{25.1}$, and its pKas were found in literature where the pKa values were used to determine α_{EDTA} ($10^{2.86}$).[99] The apparent stability constant of $Fe(SIH)_2$, $K'_{Fe(SIH)2}$, was calculated using the known concentrations of each of the components (**Equations 11-13**), the average log K'_{ex} and $K'_{Fe\text{-}EDTA}$. Values of pK_a for the hydrolysis of iron(III) were used to determine the α_{Fe}, Appendix B. The apparent stability constant for Fe-EDTA, log $K'_{Fe\text{-}EDTA}$, was thus calculated to be 16.4. The K'_{ex}, $\mathbf{K_{Fe(SIH)2}}$, and the log $\mathbf{K_{Fe(SIH)2}}$ values obtained for the complexes can be seen in **Table 3**.

$$FeEDTA + 2SIH \overset{K_{ex}}{\leftrightarrows} Fe(SIH)_2 + EDTA \qquad \text{[Eq 2]}$$

$$Fe + EDTA \overset{K_{FeEDTA}}{\leftrightarrows} FeEDTA \qquad K_{FeEDTA} = \frac{[FeEDTA]}{[Fe][EDTA]} \qquad \text{[Eq. 3, 4]}$$

$$Fe + 2SIH \overset{K_{Fe(SIH)2}}{\leftrightarrows} Fe(SIH)_2 \qquad K_{Fe(SIH)_2} = \frac{[Fe(SIH)_2]}{[Fe][SIH]^2} \qquad \text{[Eq. 5, 6]}$$

$$K'_{ex} = \frac{[Fe(SIH)_2][EDTA]}{[FeEDTA][SIH]^2} \quad \text{at pH 7.4} \qquad \text{[Eq. 7]}$$

$$K'_{ex} = \frac{K'_{Fe(SIH)2}}{K'_{FeEDTA}} \qquad \text{[Eq. 8]}$$

Where $K'_{Fe(SIH)2} = K_{Fe(SIH)2}$ at pH 7.4 [Eq. 9]

$$K'_{FeEDTA} = \frac{(\beta)(\alpha_{FeEDTA})}{\alpha_{EDTA}\alpha_{Fe}} \qquad \text{[Eq. 10]}$$

$$[Fe]_T = FeEDTA + Fe(SIH)_2 \qquad \text{[Eq. 11]}$$

$$[SIH]_T = 2Fe(SIH)_2 + SIH_{Free} \qquad \text{[Eq. 12]}$$

$$[EDTA]_T = FeEDTA + EDTA_{Free} \qquad \text{[Eq. 13]}$$

Table 3. The K'_{ex}, K'_{eff}, and the log K'_{eff}, for $Fe(SIH)_2$, $Fe(SNH)_2$, and $Fe(SPH)_2$ at pH 7.4.

	K'_{ex} (M^{-1})	$K_{Fe(SIH)2}$ (M^{-2})	log $K_{Fe(SIH)2}$
$Fe(SIH)_2$	465.7 ± 73.7	$1.17 \times 10^{19} \pm 1.9 \times 10^{18}$	$19.1 \pm 6.9 \times 10^{-2}$
$Fe(SNH)_2$	106.1 ± 7.8	$2.67 \times 10^{18} \pm 2.0 \times 10^{17}$	$18.4 \pm 3.2 \times 10^{-2}$
$Fe(HAP\text{-}INH)_2$	151.5 ± 31.4	$3.81 \times 10^{18} \pm 7.9 \times 10^{17}$	$18.6 \pm 8.8 \times 10^{-2}$

The K'_{ex}, $K_{Fe(SIH)2}$, and the log $K_{Fe(SIH)2}$ values obtained for the complexes can be seen above. Varying amounts of EDTA in a 50:50 MeOH: 10 mM HEPES/100 mM NaCl solution were used while the concentration of the chelator being analyzed was kept constant at room temperature. The absorbance at 450 nm was analyzed since Fe-EDTA has no spectral features at this wavelength.

As an example, **Figure 25** displays the absorbance of $Fe(SNH)_2$ with varying amounts of EDTA in a 50:50 MeOH: 10 mM HEPES/100 mM NaCl solution. Equivalents of EDTA to SNH have been specified within the graph. As the amount of EDTA increased in the

solution, the absorbance value decreased at 450 nm. Fe-EDTA has no spectral features at 450 nm.[51] Values of pFe for the chelators being studied, EDTA, and DFO can be found in **Table 4**.

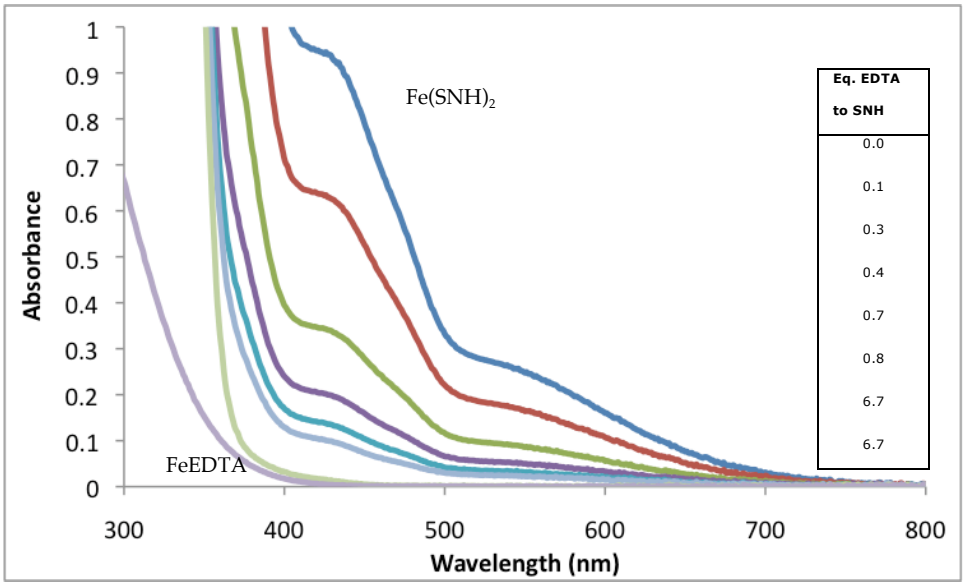

Figure 25. Absorbance of $Fe(SNH)_2$ with varying amounts of EDTA in a 50:50 MeOH: 10 mM HEPES/100 mM NaCl solution.

Table 4. pFe values for the iron(III) complexes being analyzed along with well known iron chelators.

Chelators	pFe'	pFe
SIH	20.9	27.0
SNH	20.2	26.3
HAP-INH	20.4	26.5
EDTA	-	23.4*
DFO	-	26.6**

pFe is defined as the negative log of the free iron concentration in solution at pH 7.4 with a total ligand concentration of 10 μM and total Fe concentration of 1 μM. pFe' denotes a pFe value at pH 7.4.
*pFe value of EDTA was calculated using literature values, Appendix B.
**pFe value of DFO from reference.[100]

2.3 Discussion:

2.3.1 Synthetic Strategy

A set of second-generation pro-chelators and their respective chelators have been synthesized and characterization studies on the compounds have been described. There are two possible routes for making the boronic ester pro-chelators; (1) The boronic acid hydrazone can first be made by performing a schiff base condensation with the boronic acid aldehyde/ketone and the hydrazide followed by an esterification of the boronic acid hydrazone with the diol of choice. (2) The boronic ester aldehyde/ketone can be synthesized by the esterification of the boronic acid aldehyde/ketone with the diol of choice followed by a schiff base condensation forming the boronic ester pro-chelator, **Scheme 3**. In order to optimize the yield of the final product, both routes needed to be explored. For instance, the yield for BSNH was almost doubled when route 2 was used. This can be compared to FMDOP-Bpin-H which could only be obtained by route 1.

Scheme 3. Two possible routes for the synthesis of the pro-chelators.

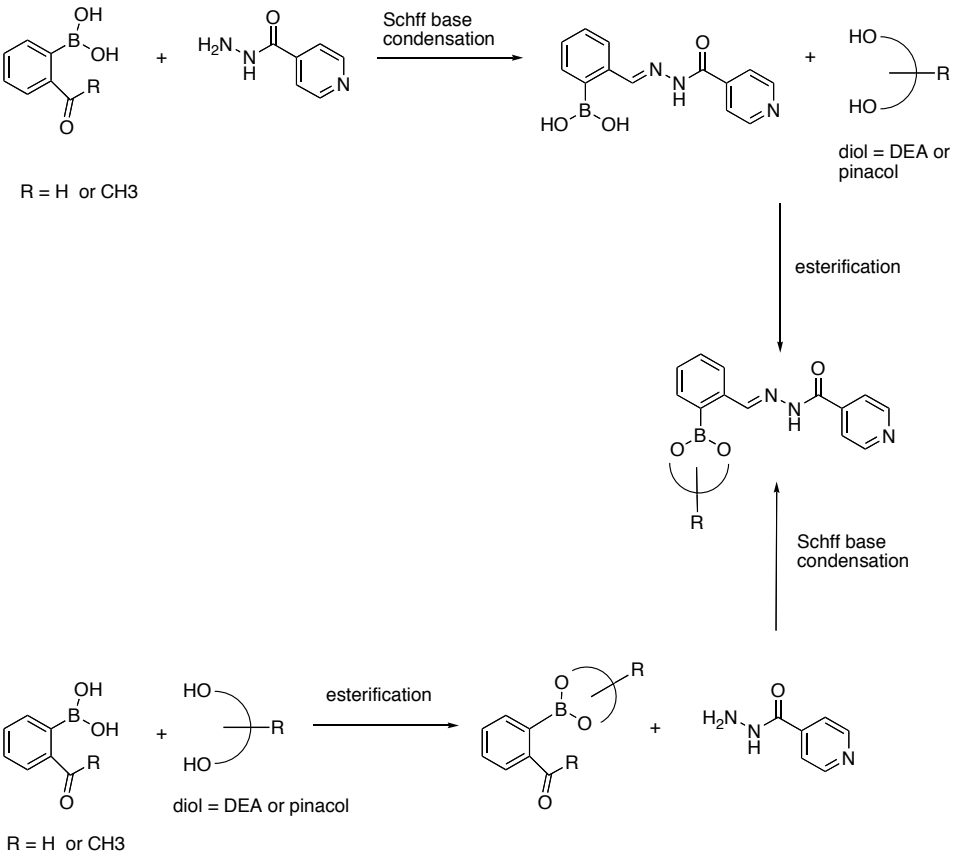

Attempts were made to synthesize the boronic ester version of HAP-INH with limited success. First the boronic acid version of the pro-chelator was synthesized, BAHAP-INH, **Figure 26**. The expected molecular weight of the boronic acid was 283.1 g/mol plus the proton by mass spectrometry (**Figure 26A**), however, a peak of 265.1 plus a proton was the main spectral feature. This peak corresponds to the structure on **Figure 26B**.

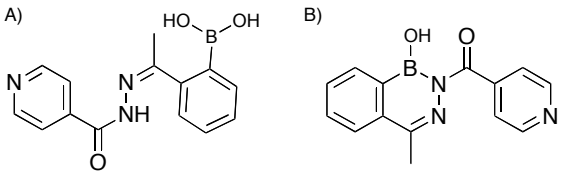

Figure 26. Possible structures of BAHAP-INH.

BAHAP-INH forms a ring between B-N and subsequently loses a water molecule in the process. Despite this fact, the esterification of the boronic acid with the diols, pinacol, and DEA were attempted at 100- 115 °C in DMF. In both cases the characteristic protons of neither the boronic esters nor the hydrazones were observed. Since the phenol oxygen and the amide nitrogen involved in iron binding are both masked in BAHAP-INH we were curious to observe whether this ligand would bind iron. One equivalent of iron was added to a solution of the chelator and the solution instantly turned dark indicating the ligand is able to bind iron.

All hope is not lost for synthesizing the boronic ester version of HAP-INH. It is possible that adding a small amount of base to the reaction mixture might force the boron to shift from its neutral trivalent form to its anionic tetravalent form, **Scheme 4**. Once the compound is in the boronate form it is likely that the B-N interaction will be weakened allowing the esterification to occur. In addition, this version should be more soluble and easier to work with.

Scheme 4. Possible route to synthesis of BHAP-INH using a selected diol.

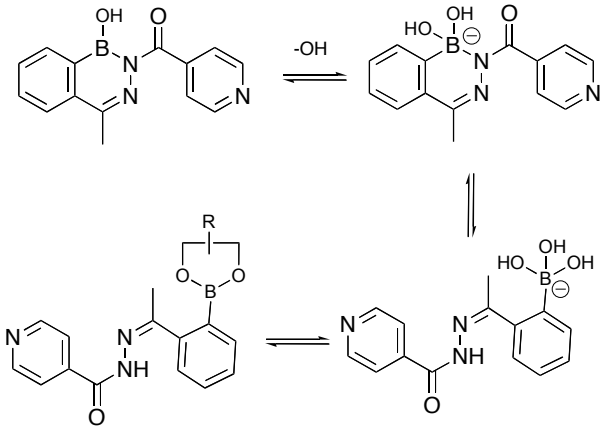

2.3.2 Stability and Solubility of the Chelators/Pro-Chelators

In the near future, our group would like to examine whether the pro-chelators mentioned in this document can be effective at protecting cells from oxidative damage. Therefore solubility and stability of these materials in biologically relevant solutions is necessary. The solubility of the pro-chelators/ chelators was determined in water, sodium phosphate buffer, 100 mM NaOH, MEM and 92% MEM: 8% DMSO. DEA-BSIH is the only pro-chelator of the set examined in this document that is soluble in water at high concentrations, 10 mM. An ^{1}H-NMR experiment was performed to assess whether the diethanolamine, DEA, on the pro-chelator was stable in water, methanol, and sodium phosphate buffer. As can be seen in **Figure 18**, after 3 and 45 hours in solutions of water, methanol, and sodium phosphate buffer no indication of unattached DEA is visible by ^{1}H-NMR spectra. This indicates that the DEA diol is bound to the boron on the pro-chelator.

Dissolving some of the pro-chelators/chelators directly in MEM was problematic. Although BSIH is soluble in MEM at 200 μM, neither BSPH nor FMDOP-Bpin-IH was soluble up to 50 μM. In order to get all the chelators and pro-chelators dissolved in the same solvent system, a solution of 92% MEM: 8% DMSO was used since both the chelators and pro-chelators were soluble in DMSO. All of the pro-chelators examined were soluble in the 92% MEM: 8% DMSO solution, however, once MEM was introduced to the chelator DMSO solutions, SIH, SPH, and FMDOP-IH came out of solution. Clearly, another method needed to be employed.

Previously, our group has used solutions of 100 mM NaOH to dissolve pro-chelators/chelators to make less concentrated solutions in MEM and sodium phosphate buffer. Solutions of 1 mM pro-chelators/chelators were made in 100 mM NaOH and all were soluble. The stability of the compounds was examined in the NaOH solution to

find out if the pro-chelators/chelators can be stored in this solution for at least 2 days if frozen without hydrolyzing into their hydrazide and aldehyde/ketone counterparts. While BSIH, BSNH, and BSPH show minimal change in their UV spectra, DEA-BSIH shows no change in the spectra even after sitting at room temperature for 4 h. However, FMDOP-Bpin-IH shows some spectral change indicating that one would want to make up fresh solutions daily when working with it. In MEM at pH 7.4 the pro-chelators showed minimal changes in their UV spectra while the chelators, SNH, SPH, and FMDOP-IH showed dramatic changes in their spectra. HAP-INH showed minimal UV spectral changes. This suggests that adding a methyl group to the imine carbon of SIH stabilizes the hydrazone in MEM.

2.3.3 Pro-Chelator Rates of Activation: The Oxidation of the Pro-chelator to Chelator

Rate studies of oxidation were performed for BSIH and DEA-BSIH using various concentrations of H_2O_2 under pseudo first order reaction conditions. The second order rate constant, k, of BSIH was previously determined to be 0.053 M^{-1} s^{-1} at 300 nm.[51] Using the corrected value for the ln of absorbance at 380 nm, **Equation 1**, the second order rate constants were determined to be k=0.032 M^{-1} s^{-1} for BSIH and k=0.023 M^{-1} s^{-1} for DEA-BSIH . Therefore changing the diol mask from pinnacol to diethanolamine caused little change in the rate of unmasking. It is also important to note that SIH was monitored for three hours in the presence of H_2O_2 to determine whether the peroxide would induce degradation of the chelator. No change in absorbance was observed over the 3 hour course.

2.3.4 Apparent Stability Constants of Chelators at pH 7.4 with Iron(III)

EDTA is a well known metal chelator with known spectral features and an affinity for iron(III) which has been well documented. Therefore, it was a good choice

for the competition between iron(III) and the new chelators being characterized. To obtain an apparent stability constant, also known at the conditional or effective stability constants, a buffered solution at pH 7.4 at room temperature was employed. The log of the apparent stability constants, log K', for $Fe(SIH)_2$, $Fe(SNH)_2$, and $Fe(HAP\text{-}INH)_2$ were found to be 19.1, 18.4, 18.6, respectively, at the specified conditions. However, it is often more useful to compare pFe values ($-\log[Fe_{aq}^{3+}]$) than directly comparing apparent stability constants to different ligands because of differences in pKa's and denticities. A pFe value measures the amount of uncomplexed iron that would be available at typical conditions of pH 7.4 with total ligand and iron concentrations of 10 μM and 1 μM, respectively. Values of pFe for SIH have been reported previously and range from 23-50. Issues with solubility and hydrolysis of the chelator at high and low pH values during potentiometric titrations could explain the wide ranges of pFe values reported for SIH. Using the technique of a competition between our ligands and EDTA, values of pFe for SIH, SNH, and HAP-INH were found to be 27.0, 26.3, and 26.5, respectively. For comparison, pFe values of EDTA and DFO are 23.4 and 26.6, respectively. Between the chelators analyzed herein, changing the position of the nitrogen of the aroyl ring to the meta position and adding a methyl group to the imine carbon of SIH seem to have minimal effects on the stability of the metal complexes.

2.3.5 Summary and Conclusions

A group of second generation iron pro-chelators have been described which are derivatives of the parent compound, BSIH. These masked chelators can potentially reveal high affinity metal ligands when oxidized by H_2O_2. Unlike traditional iron chelators, which can disrupt iron homeostasis, these pro-chelators have a protective mask consisting of various boronic esters that react and reveal a phenolic oxygen selectively by H_2O_2. Compared to the first generation pro-chelator/chelator pair,

BSIH/SIH, changes have been made to the ligands to study solubility, changes in iron binding stability, and rates of oxidation. Dissolving the pro-chelators/chelators in base before further diluting in cell culture media or buffer was found to increase the solubility of the compounds significantly. Concentrations as low as 50 μM were achieved whereas without adding base most would not go into solution or would precipitate out. A noteworthy exception was the DEA-BSIH prochelator. This BSIH derivative was soluble in water even at 10 mM. The boronic ester of this prochelator showed stability in water, methanol, and 20 mM sodium phosphate buffer even after 45 hours in solution.

Upon further examination of BSIH a peak at 8.5 ppm in the ^{1}H- NMR, which was originally thought to be a contaminate, the peak turned out to be a proton corresponding to the boronate version of BSIH. Depending on the amount of water in the sample as well as the pH of a solution, this peak will vary in size.

Kinetics of oxidation of BSIH and DEA-BSIH were performed in H_2O_2 and minimal differences were found in the rates of unmasking. BSIH was also exposed to tert-butyl hydroperoxide with no reaction observed.

The apparent stability constants and pFe values of SIH, SNH, and HAP-INH were determined and found to be comparable to DFO. Changing the position of the nitrogen of the aroyl ring to the meta position (SNH) and adding a methyl group to the imine carbon of SIH (HAP-INH) seem to have minimal effects on the stability of the metal complexes.

Appendix A

Determination of stability of pro-chelators/chelators in 100 mM NaOH, conditions needed for solubility purposes

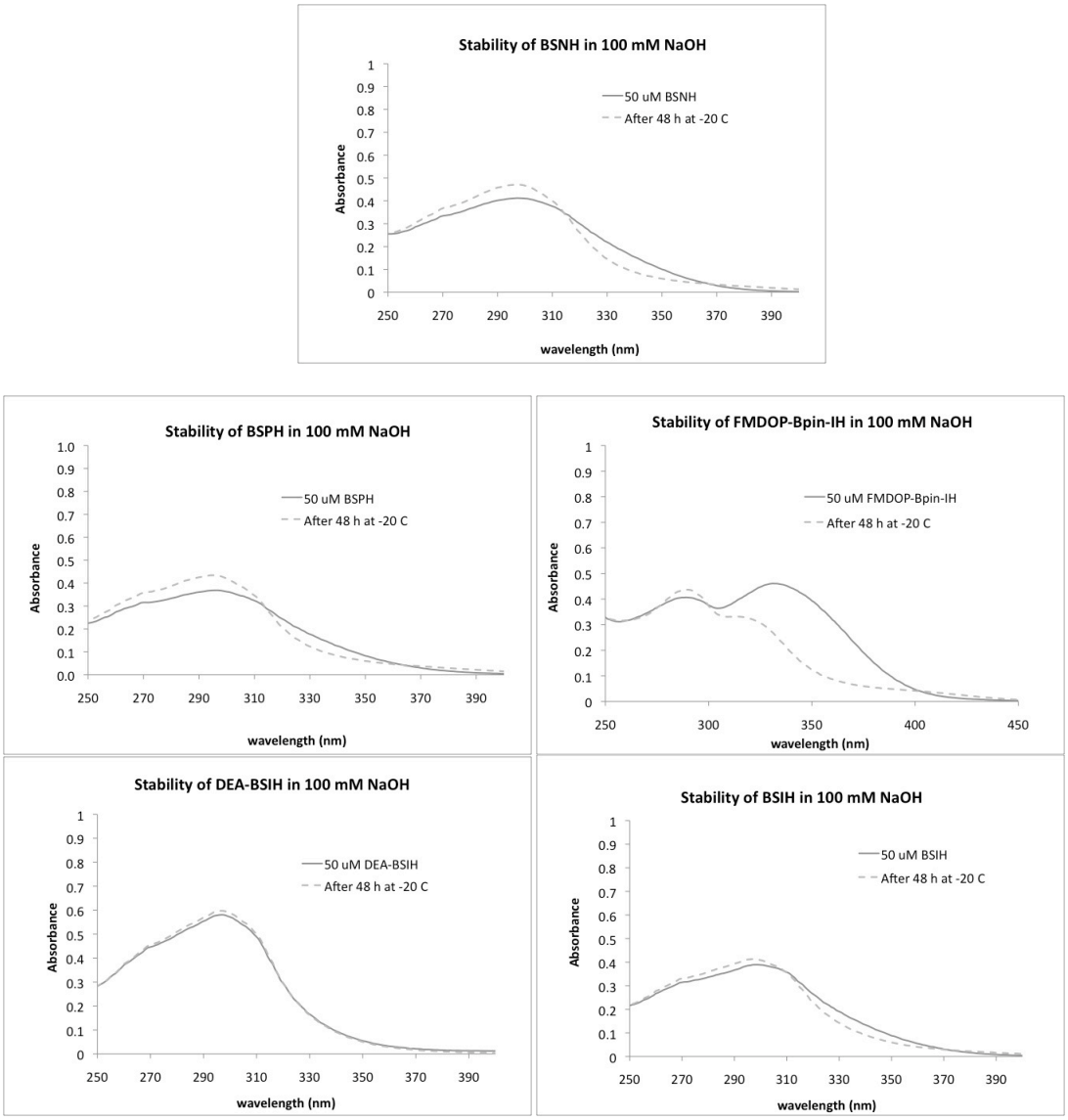

Figure 27. UV-vis spectra of 50 µM solutions of FMDOP-Bpin-IH, DEA-BSIH, BSNH, BSPH, and BSIH in 100 mM NaOH before and after freezing at -20 C. Spectra of FMDOP-Bpin-IH and DEA-BSIH can also be found in the document in Figure 20.

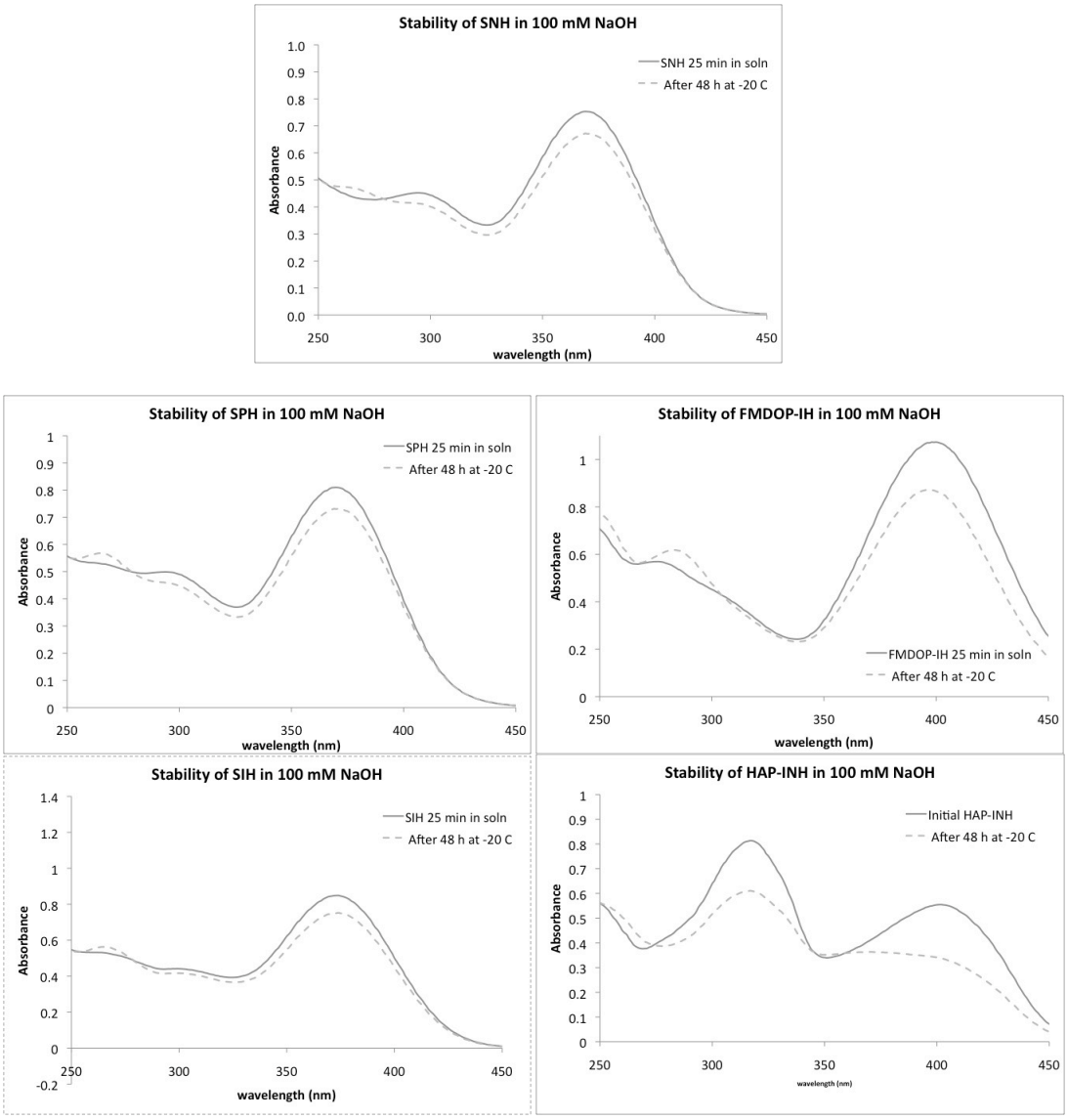

Figure 28. UV-vis spectra of 50 µM solutions of SNH, SPH, SIH, FMDOP-IH and HAP-INH in 100 mM NaOH before and after freezing at -20 C.

Determination of stability in minimal essential media, MEM, conditions for future cell studies

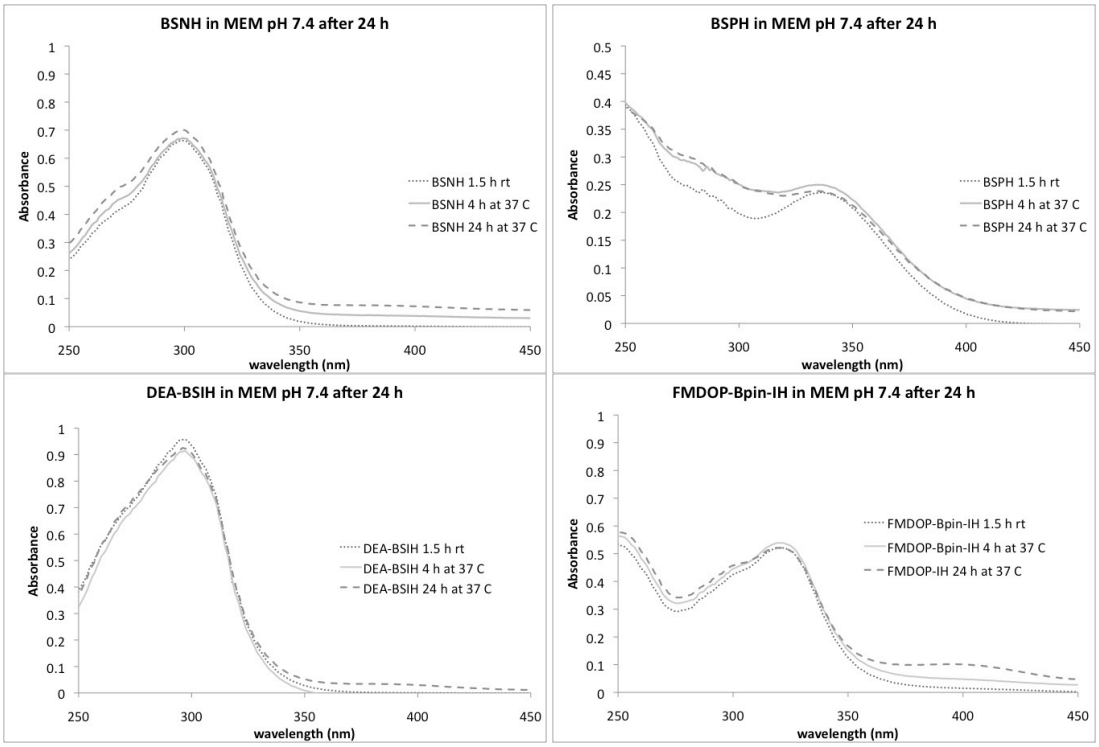

Figure 29. 50 µM solutions of the pro-chelators, BSNH, BSPH, DEA-BSIH, and FMDOP-Bpin-IH in MEM at pH 7.4 and 37 °C. Spectra of DEA-BSIH can also be found in the document in Figure 21.

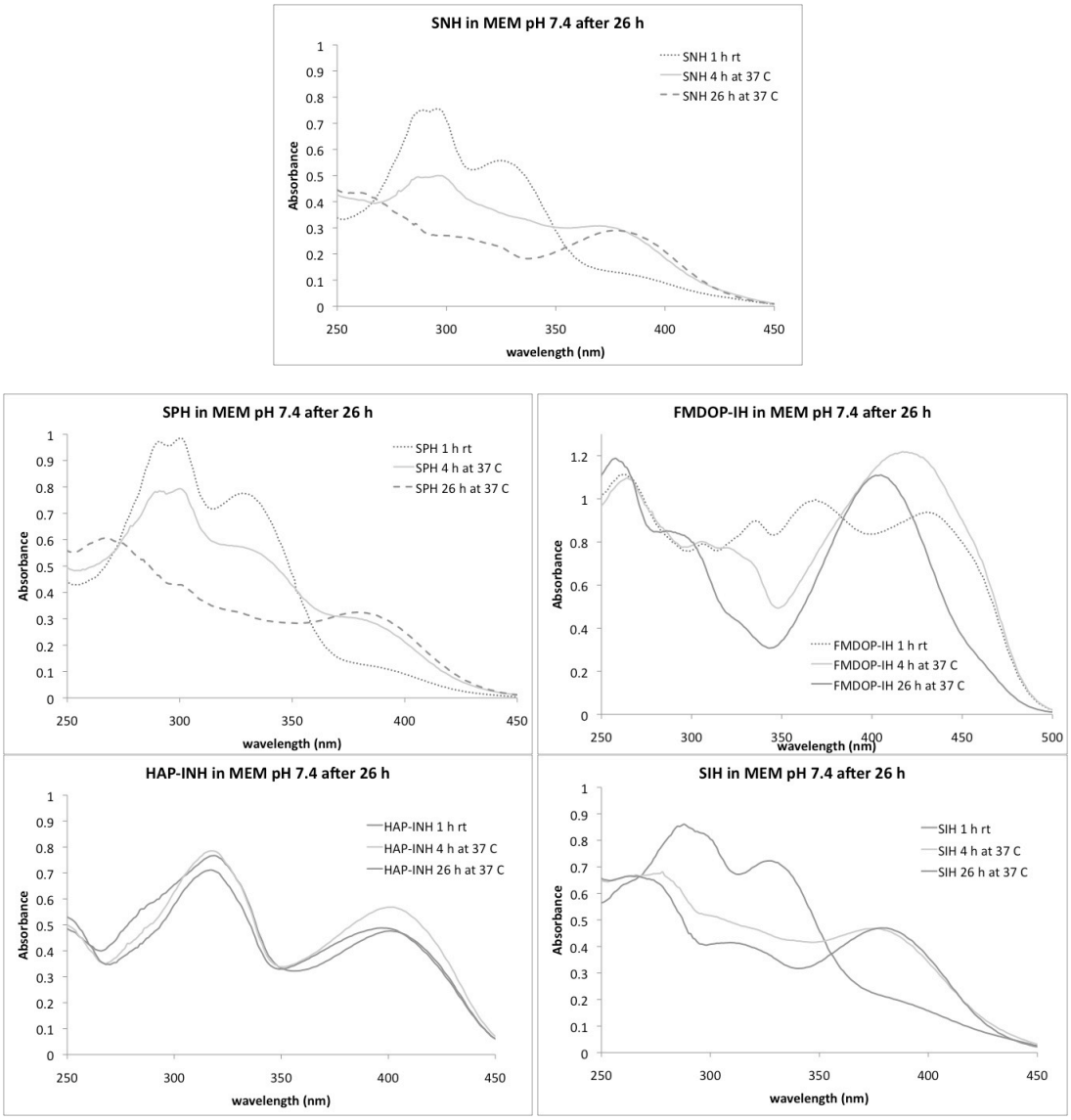

Figure 30. 50 µM solutions of the chelators, SNH, SPH, FMDOP-IH, and HAP-INH in MEM at pH 7.4 and 37 °C. Spectra of SIH can also be found in the document in Figure 21.

[1]H-NMR Spectra of Chelators and Pro-Chelators

H^1-NMR of SPH in d_6-DMSO

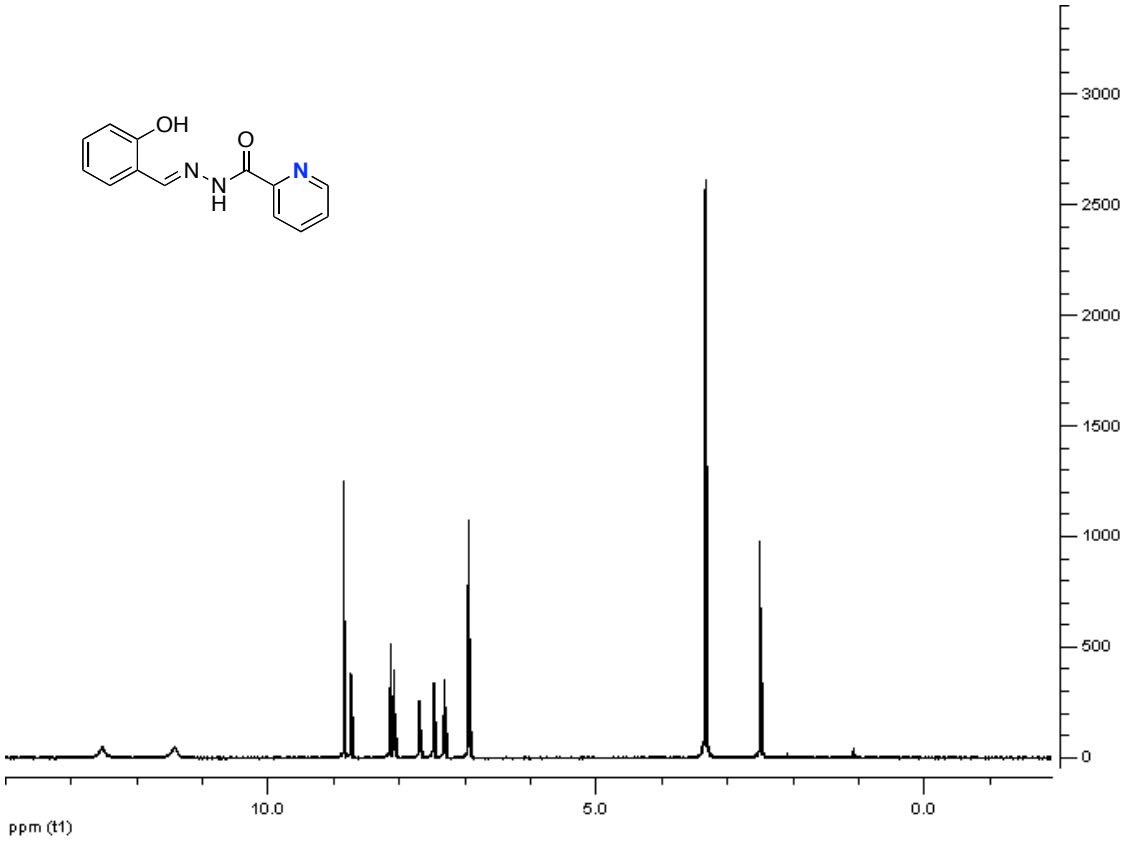

H^1-NMR of SNH in d_6-DMSO

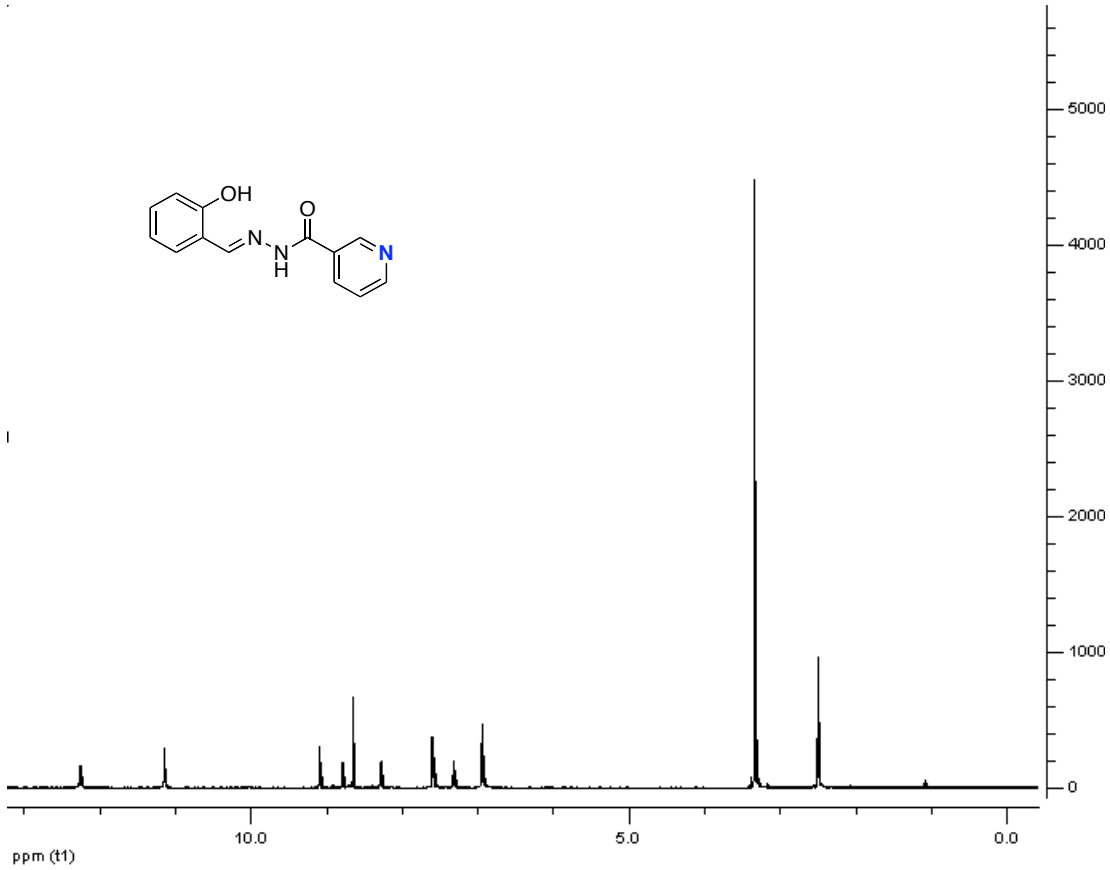

H^1-NMR of HAP-INH in d_6-DMSO

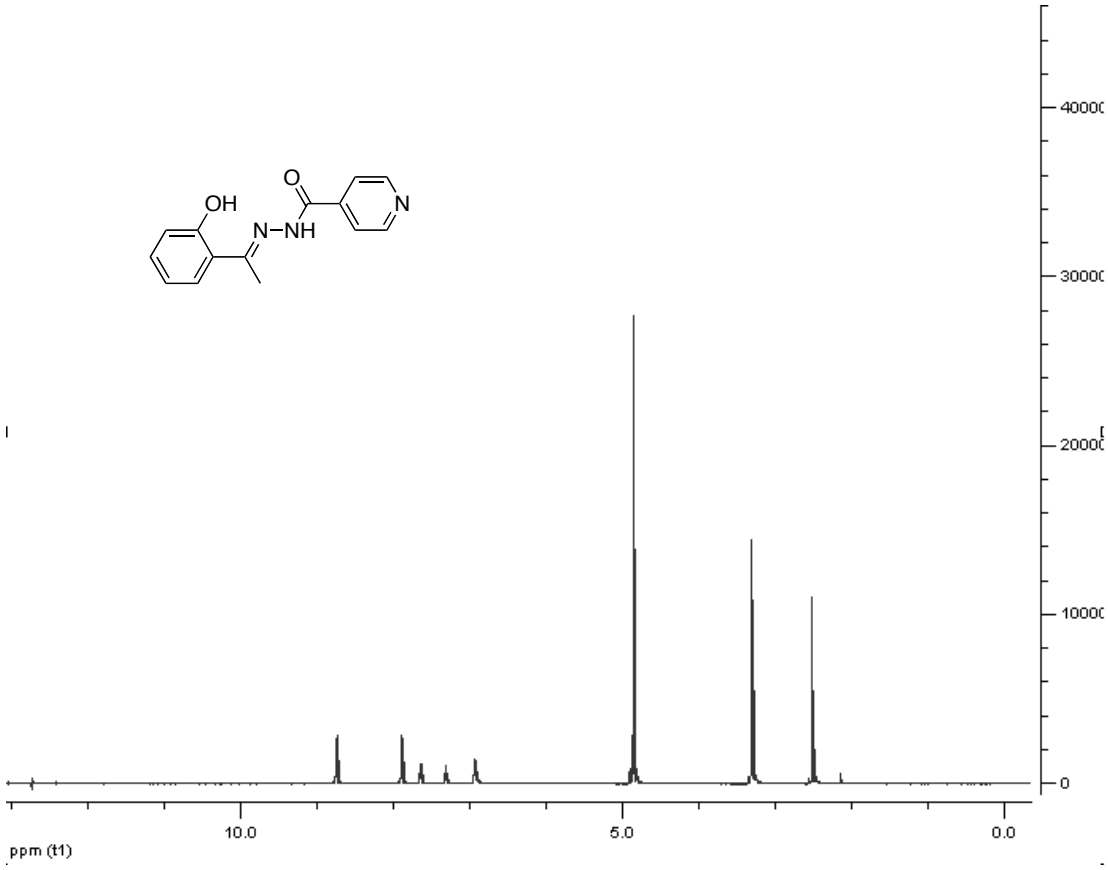

H^1-NMR of FMDOP-IH in d_6-DMSO

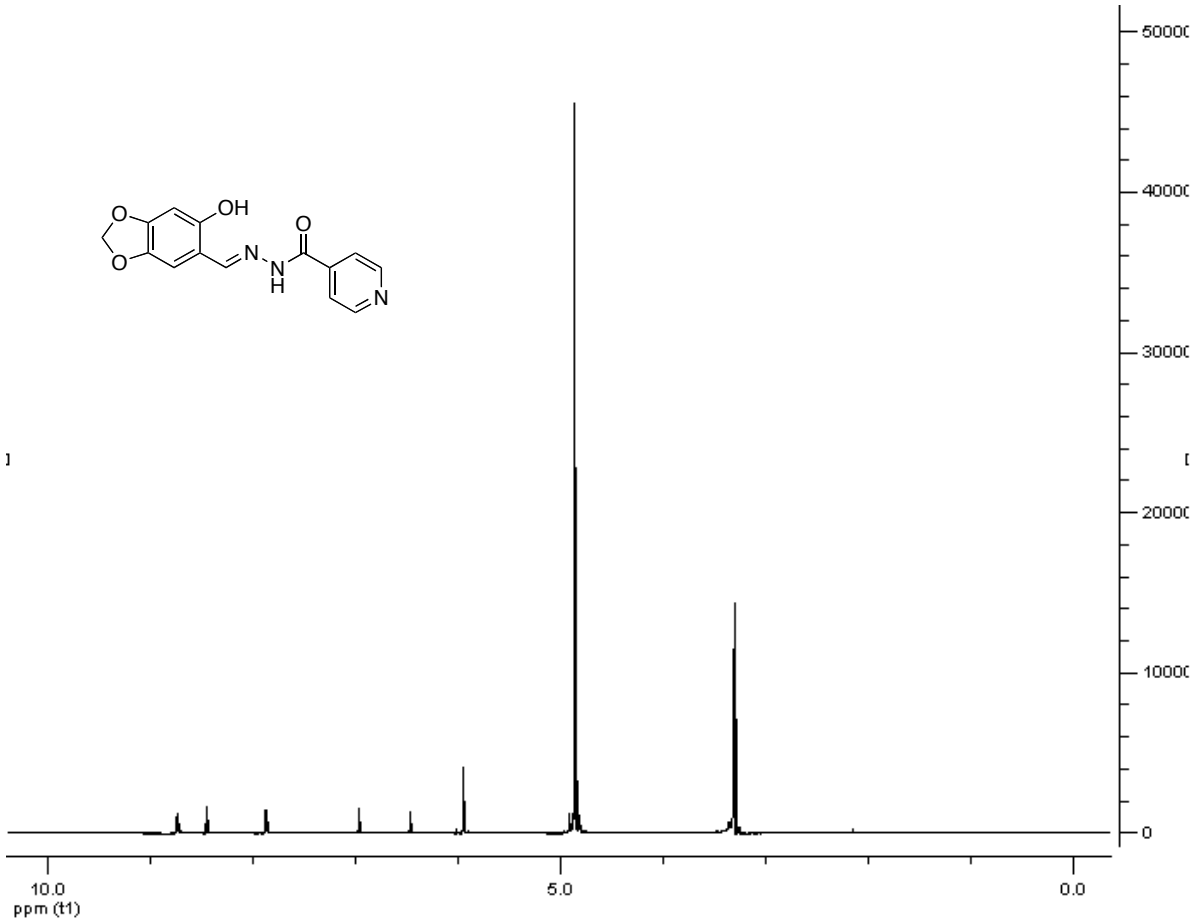

H^1-NMR of BSNH in d_6-DMSO

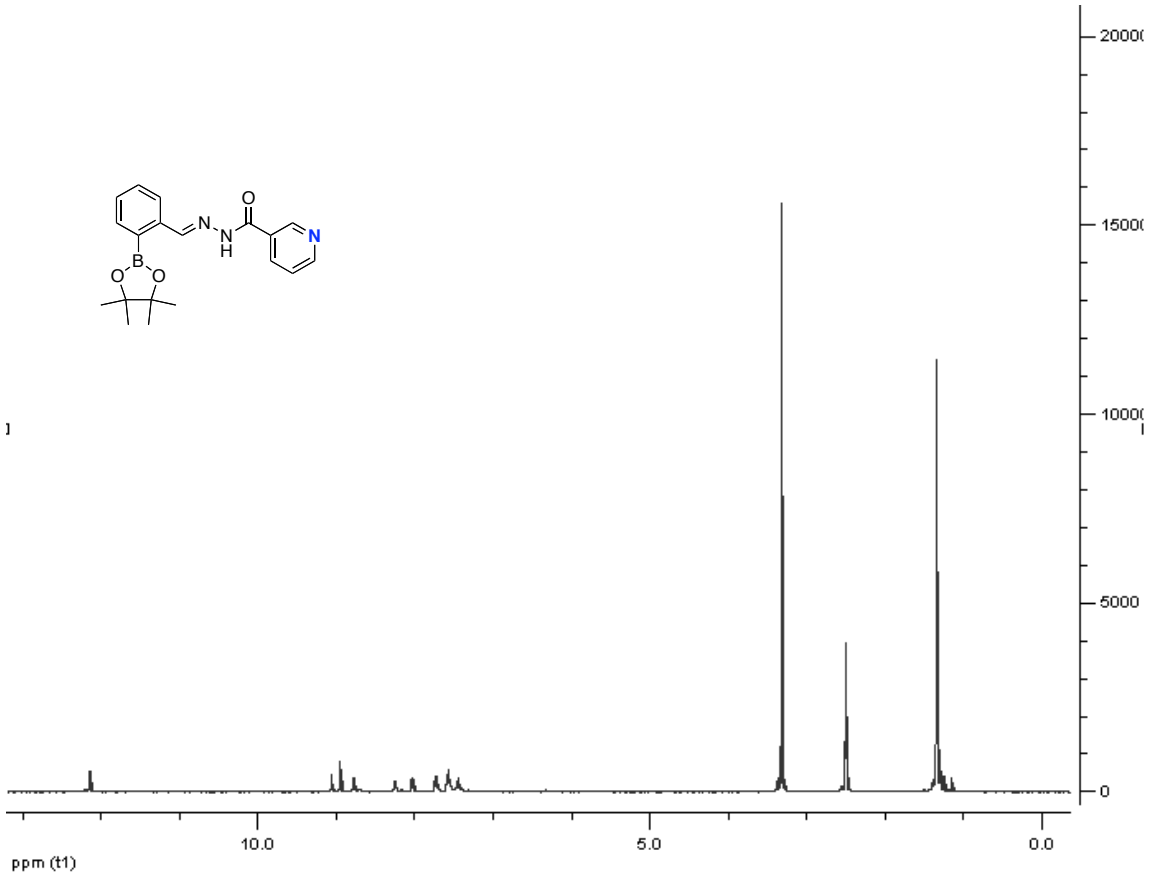

H^1-NMR of BSPH in d_6-DMSO

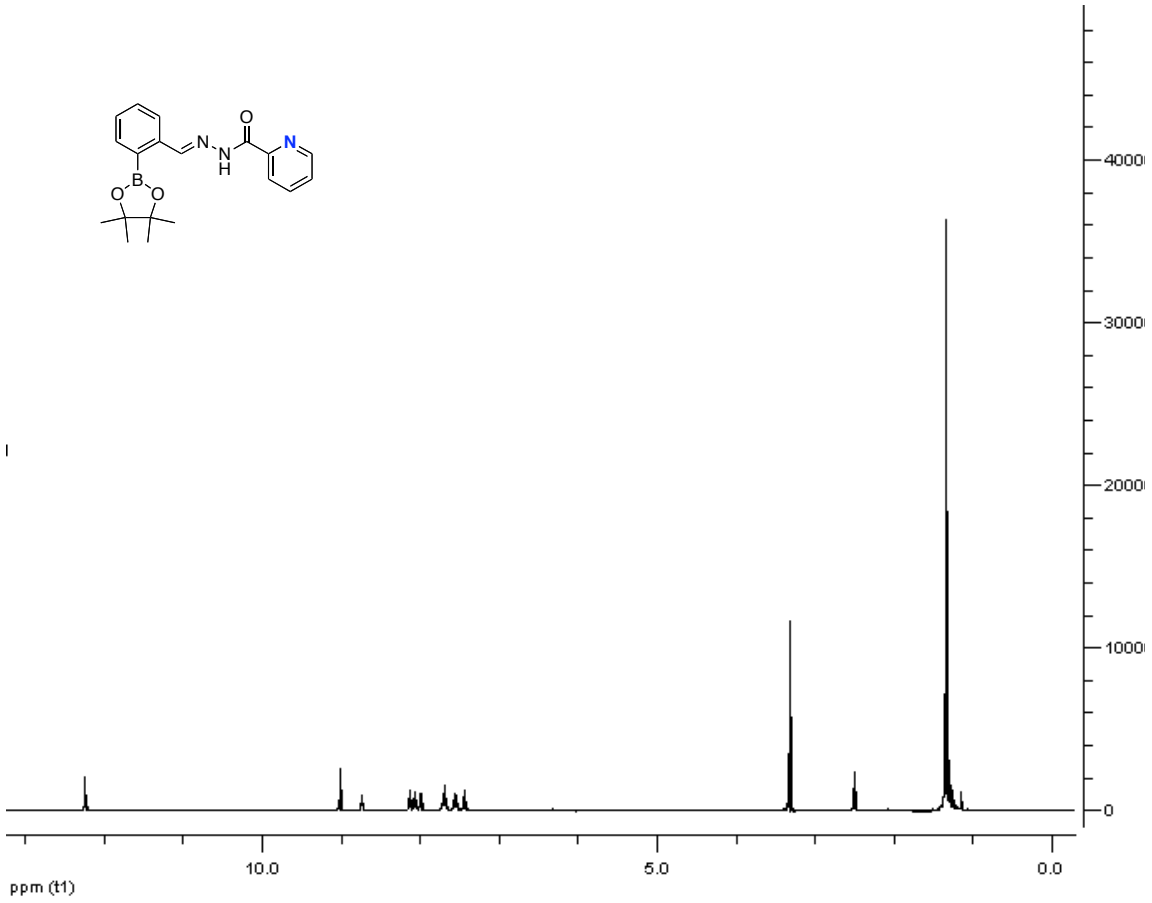

H^1-NMR of DEA-BSIH in d_6-DMSO

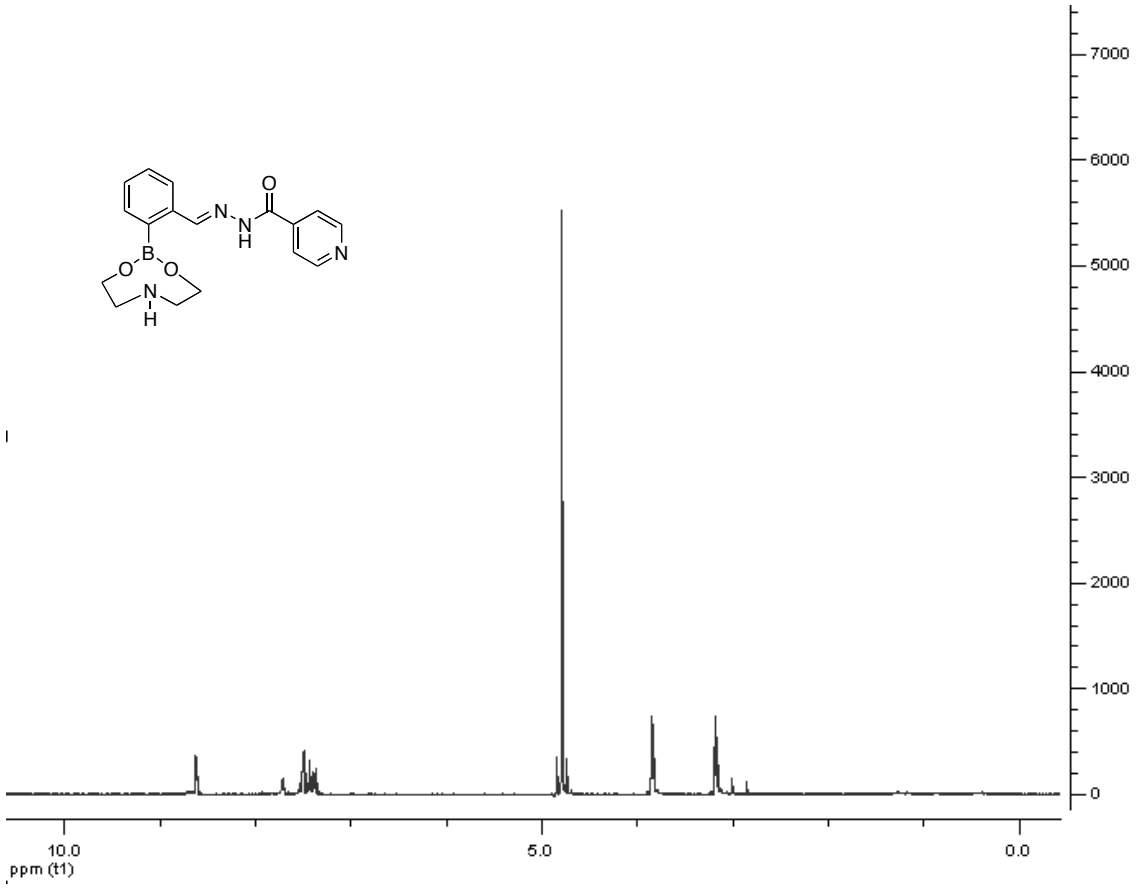

H^1-NMR of FMDOP-Bpin-IH in d_6-DMSO

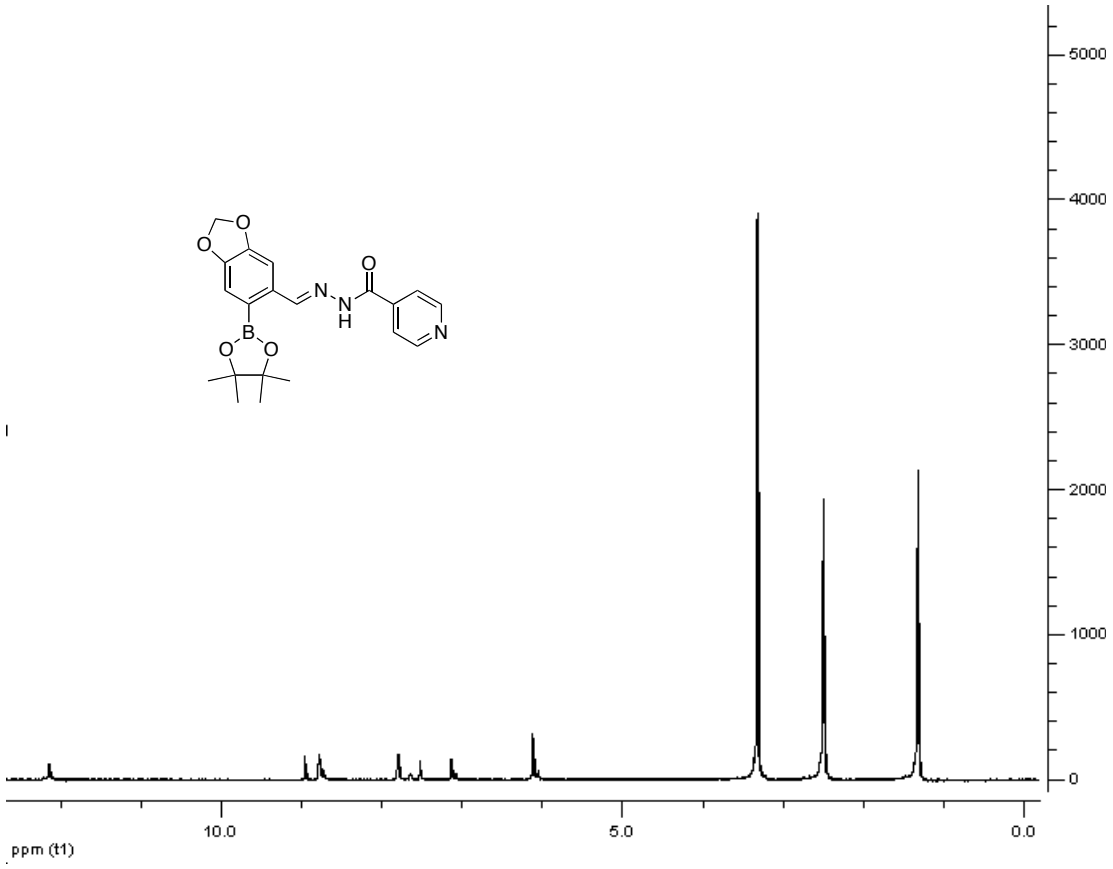

Appendix B

Determining a pFe value

$$M + nL \leftrightarrows ML_n \qquad K_{ML_n} = \frac{[(ML_n)]}{[M][L]^n} \qquad \text{[Eq. 1, 2]}$$

Equation 1 shows the chemical equilibrium of a metal and a ligand with n binding sites. The stability constant, K, is defined in equation 2. At constant ionic strength and pH an apparent stability constant, also known as a conditional or effective stability constant, can be defined, equation 3:

$$K'_{ML_n} = K_{ML_n}\frac{\alpha_{ML}}{\alpha_L\alpha_M} = \frac{[(ML_n)']}{[M'][L']^n} \qquad \text{[Eq. 3]}$$

where K'_{ML_n} is the conditional stability constant, K_{ML_n} is the stability constant for the complex, [M′] is the free metal (metal not bound to the ligand), $[L']^n$ is the concentration of free ligand, and $[(ML_n)']$ is concentration of complex. The value of n denotes how many binding sites are available on the ligand for metal binding; ie. In the case of a bis complex, n = 2.

By definition pFe equals the concentration of the free uncomplexed metal and therefore one must solve for [M′]. Equation 3 can be rearranged to solve for $[M']^{-1}$ and equation 4 is obtained.

$$\frac{1}{[M']} = K_{ML_n}\frac{\alpha_{ML_n}}{\alpha_L\alpha_M} \bullet \frac{[L']^n}{[(ML_n)']} \qquad \text{[Eq. 4]}$$

The α values are called side reaction coefficients (fraction of uncomplexed ligand/ metal/ ML) defined by equations 5- 10:

$$\alpha_{ML_n} = \frac{[(ML_n)']^n}{[ML_n]^n} \qquad [(ML_n)'] = \alpha_{ML_n}[ML_n]^n \qquad \text{[Eq. 5, 6]}$$

$$\alpha_M = \frac{[M']}{[M]} \qquad [M'] = \alpha_M [M] \qquad \text{[Eq. 7, 8]}$$

$$\alpha_{Ln} = \frac{[L_n']^n}{[L_n]^n} \qquad [L_n'] = \alpha_{L_n} [L_n]^n \qquad \text{[Eq. 9, 10]}$$

Solving for pM′, equation 4 can be expressed as equation 11.

$$pM' = \log K_{ML_n} - \log \alpha_M + \log \frac{\alpha_{ML_n}}{\alpha_L} + \log \frac{[L']^n}{[(ML_n)']} \qquad \text{[Eq. 11]}$$

Where pM′ is equal to the following (Eq. 12):

$$pM' = \log[M']^{-1} = -\log[M'] \qquad \text{[Eq. 12]}$$

The log of K'_{ML_n} can be substituted into equation 11 to yield equation 13.

$$pM' = \log K'_{ML_n} + \log \frac{[L']^n}{[(ML_n)']} \qquad \text{[Eq. 13]}$$

To obtain pM, the log α_M must be added back in, equation 14.

$$pM = pM' + \log \alpha_M \qquad \text{[Eq. 14]}$$

Determining pFe value of EDTA at pH 7.4

Fe + EDTA ⇆ Fe-EDTA at pH 7.4 [Eq. 15]

The conditional stability constant of the Fe-EDTA equilibrium reaction can be seen in equation 16.

$$K'_{FeEDTA} = \frac{[FeEDTA]}{[Fe][EDTA]} = \frac{(\beta)(\alpha_{FeEDTA})}{(\alpha_{EDTA})(\alpha_{Fe^{3+}})} \quad \text{[Eq. 16]}$$

Where K'_{FeEDTA} is the apparent stability constant of FeEDTA at pH 7.4, β is the conditional (pH independent) constant, and the α values are the fraction of uncomplexed ligand/metal. The value of β is $10^{25.1}$.[99]

The following equations are used to determine how to calculate the α values needed to obtain the K'_{FeEDTA} at pH 7.4.

α_{EDTA} Calculations:

		pK_a values at 25 C and I= 0.15 [99]	
H + EDTA ⇆ EDTA-H	$\frac{[HL]}{[H][L]}$	10.27	[Eq. 17,18]
H + EDTA-H ⇆ EDTA-H_2	$\frac{[H_2L]}{[HL][H]}$	6.16	[Eq. 19,20]
H + EDTA-H_2 ⇆ EDTA-H_3	$\frac{[H_3L]}{[H_2L][H]}$	2.67	[Eq. 21,22]
H + EDTA-H_3 ⇆ EDTA-H_4	$\frac{[H_4L]}{[H_3L][H]}$	2.00	[Eq. 23,24]

Where α_{EDTA} can be defined as the following in equation 25:

$$\alpha_{EDTA} = \frac{[L]}{[L]} + \frac{[HL]}{[L]} + \frac{[H_2L]}{[L]} + \frac{[H_3L]}{[L]} + \frac{[H_4L]}{[L]} \quad \text{[Eq. 25]}$$

Equation 25 can be reduced to equation 26.

$$\alpha_{EDTA} = 1 + 10^{(pK_1 - pH)} + 10^{(pK_1 + pK_2 - 2pH)} + 10^{(pK_1 + pK_2 + pK_3 - 3pH)} + 10^{(pK_1 + pK_2 + pK_3 + pK_4 - 4pH)}$$ [Eq. 26]

Using the pK_a values mentioned above, α_{EDTA} equal 784.97 and the log α_{EDTA} equal 2.89.

$\alpha_{Fe^{3+}}$ Calculations:

		pK_a values[101]	
$Fe(OH_2)_6 \leftrightarrows Fe(OH_2)_5(OH) + H$	$\frac{[H][Fe(OH)]}{[Fe]}$	2.56	[Eq. 27, 28]
$Fe(OH_2)_5(OH) \leftrightarrows Fe(OH_2)_4(OH)_2 + H$	$\frac{[H][Fe(OH)_2]}{[FeOH]}$	6.19	[Eq. 29, 30]
$Fe(OH_2)_4(OH) \leftrightarrows Fe(OH_2)_3(OH)_3 + H$	$\frac{[H][Fe(OH)_3]}{[Fe(OH)_2]}$	10	[Eq. 31, 32]

Where $\alpha_{Fe^{3+}}$ can be defined as the following in equation 33:

$$\alpha_{Fe^{3+}} = \frac{[Fe]}{[Fe]} + \frac{[FeOH]}{[Fe]} + \frac{[Fe(OH)_2]}{[Fe]} + \frac{[Fe(OH)_3]}{[Fe]} + \ldots$$ [Eq. 33]

$$\alpha_{Fe^{3+}} = 1 + 10^{(pH - pK_1)} + 10^{(2pH - pK_1 - pK_2)} + 10^{(3pH - pK_1 - pK_2 - pK_3)}$$ [Eq. 34]

Using the pK_a values mentioned above, $\alpha_{Fe^{3+}}$ equals 1.19×10^6 and the log $\alpha_{Fe^{3+}}$ equals 6.08.

α_{FeEDTA} Calculations:

		pK_a values[102]	
FeEDTA + H ⇆ FeEDTA-H	$\frac{[MHL]}{[ML][H]}$	1.3	[Eq. 35,36]
FeEDTA(OH) + H ⇆ FeEDTA	$\frac{[ML]}{[M(OH)L][H]}$	7.49	[Eq. 37,38]
$FeEDTA(OH)_2$ + H ⇆ Fe(OH)EDTA	$\frac{[M(OH)L]}{[M(OH)_2L][H]}$	9.41	[Eq. 39, 40]

Where α_{FeEDTA} can be defined as the following in equation 41:

$$\alpha_{FeEDTA} = \frac{[FeL]}{[FeL]} + \frac{[FeHL]}{[FeL]} + \frac{[Fe(OH)]}{[FeL]} + \frac{[Fe(OH)_2L]}{[FeL]} \quad \text{[Eq. 41]}$$

$$\alpha_{FeEDTA} = 1 + 10^{(pK_1 - pH)} + 10^{(pH - pK_2)} + 10^{(2pH - pK_2 + pK_3)} \quad \text{[Eq. 42]}$$

Using the pK_a values mentioned above, α_{FeEDTA} equals 1.82 and the log α_{FeEDTA} equals 0.260.

Log K'$_{FeEDTA}$ Determination

Once all the α values have been determined, log K'_{FeEDTA} was calculated by taking the log of equation 16 and found to be 16.4.

pFe for Fe-EDTA

$$pFe' = \log K'_{FeEDTA} + \log \frac{[EDTA']}{[(FeEDTA)']}$$

pFe is defined as the negative log of the free iron concentration in solution at pH 7.4 with a total ligand concentration of 10 μM and total Fe concentration of 1 μM. Therefore a concentration of 1 μM is used for [(FeEDTA)'] and 9 μM for [EDTA']. To obtain pFe values of pFe' and log α_M were inserted in equation 14 and the pFe was determined to be 23.4.

References

1. Andrews, N. C.; Schmidt, P. J., Iron Homeostasis. *Ann. Rev. Physiol.* **2007,** *69* (1), 69-85.

2. Cousins, R. J.; Liuzzi, J. P.; Lichten, L. A., Mammalian Zinc Transport, Trafficking, and Signals. *J. Biol. Chem.* **2006,** *281* (34), 24085-24089.

3. Kim, B.-E.; Nevitt, T.; Thiele, D. J., Mechanisms for copper acquisition, distribution and regulation. *Nat Chem Biol* **2008,** *4* (3), 176-185.

4. Pierre, J. L.; Fontecave, M., Iron and activated oxygen species in biology: The basic chemistry. *Biometals* **1999,** *12*, 195-199.

5. Prousek, J., Fenton chemistry in biology and medicine *.(Henry John Horstman Fenton). *Pure Appl. Chem.* **2007,** *79* (12), 2325(14).

6. Faller, P.; Hureau, C., Bioinorganic chemistry of copper and zinc ions coordinated to amyloid-[small beta] peptide. *Dalton Transactions* **2009,** (7), 1080-1094.

7. Roychaudhuri, R.; Yang, M.; Hoshi, M. M.; Teplow, D. B., Amyloid {beta}-Protein Assembly and Alzheimer Disease. *Journal of Biological Chemistry* **2009,** *284* (8), 4749-4753.

8. Castellani, R. J.; Honda, K.; Zhu, X. W.; Cash, A. D.; Nunomura, A.; Perry, G.; Smith, M. A., Contribution of redox-active iron and copper to oxidative damage in Alzheimer disease. *Ageing Research Reviews* **2004,** *3* (3), 319-326.

9. Gaggelli, E.; Kozlowski, H.; Valensin, D.; Valensin, G., Copper Homeostasis and Neurodegenerative Disorders (Alzheimer's, Prion, and Parkinson's Diseases and Amyotrophic Lateral Sclerosis). *Chem. Rev.* **2006,** *106* (6), 1995-2044.

10. Crichton, R. R.; Dexter, D. T.; Ward, R. J., Metal based neurodegenerative diseases--From molecular mechanisms to therapeutic strategies. *Coordination Chemistry Reviews* **2008,** *252* (10-11), 1189-1199.

11. Crichton, R. R.; Ward, R. J., *Metal-based neurodegeneration: from molecular mechanisms to therapeutic strategies*. Wiley: Hoboken, NJ, 2006.

12. Halliwell, B., Oxidative stress and neurodegeneration: where are we now? *J. Neurochem.* **2006,** *97* (6), 1634-1658.

13. Barnham, K. J.; Masters, C. L.; Bush, A. I., Neurodegenerative diseases and oxidative stress. *Nat. Rev. Drug Disc.* **2004,** *3* (3), 205-214.

14. Zecca, L.; Youdim, M. B. H.; Riederer, P.; Conner, J. R.; Crichton, R. R., Iron, brain aging and neurodegenerative disorders. *Nat. Rev. Neurosci.* **2004,** *5*, 863-873.

15. Kell, D., Iron behaving badly: inappropriate iron chelation as a major contributor to the aetiology of vascular and other progressive inflammatory and degenerative diseases. *BMC Medical Genomics* **2009,** *2* (1), 2.

16. Gaeta, A.; Hider, R. C., The crucial role of metal ions in neurodegeneration: the basis for a promising therapeutic strategy. *British Journal of Pharmacology* **2005,** *146* (8), 1041-1059.

17. Richardson, D. R., Novel chelators for central nervous system disorders that involve alterations in the metabolism of iron and other metal ions. *Annals of the New York Academy of Sciences* **2004,** *1012*, 326-341.

18. Youdim, M. B. H.; Stephenson, G.; Ben Shachar, D., Ironing iron out in Parkinson's disease and other neurodegenerative diseases with iron chelators - A lesson from 6-hydroxydopamine and iron chelators, desferal and VK-28. *Annals of the New York Academy of Sciences* **2004,** *1012*, 306-325.

19. Madsen, E.; Gitlin, J. D., Copper and Iron Disorders of the Brain. *Annu. Rev. Neurosci.* **2007,** *30* (1), 317-337.

20. Tam, T. F.; Leung-Toung, R.; Li, W. R.; Wang, Y. S.; Karimian, K.; Spino, M., Iron chelator research: Past, present, and future. *Current Medicinal Chemistry* **2003,** *10* (12), 983-995.

21. Kalinowski, D. S.; Richardson, D. R., The Evolution of Iron Chelators for the Treatment of Iron Overlad Disease and Cancer. *Pharmacol. Rev.* **2005,** *57*, 547-583.

22. Kontoghiorghes, G. J.; Pattichis, K.; Neocleous, K.; Kolnagou, A., The design and development of deferiprone (L1) and other iron chelators for clinical use: Targeting methods and application prospects. *Current Medicinal Chemistry* **2004,** *11* (16), 2161-2183.

23. Liu, Z. D.; Hider, R. C., Design of iron chelators with therapeutic application. *Coordination Chemistry Reviews* **2002,** *232* (1-2), 151-171.

24. Liu, Z. D.; Kayyali, R.; Hider, R. C.; Porter, J. B.; Theobald, A. E., Design, synthesis, and evaluation of novel 2-substituted 3-hydroxypyridin-4-ones: Structure-activity investigation of metalloenzyme inhibition by iron chelators. *Journal of Medicinal Chemistry* **2002,** *45* (3), 631-639.

25. Liu, Z. D.; Lockwood, M.; Rose, S.; Theobald, A. E.; Hider, R. C., Structure-activity investigation of the inhibition of 3-hydroxypyridin-4-ones on mammalian tyrosine hydroxylase. *Biochem. Pharmacol.* **2001,** *61* (3), 285-290.

26. Waldmeier, P. C.; Buchle, A. M.; Steulet, A. F., Inhibition of catechol-*o*-methyltransferase (COMT1) as well as tyrosine and tryptophan hydroxylase by the orally-active iron chelator, 1,2-dimethyl-3-hydroxypyridin-4-one (L1, CP20), in rat brain in vivo. *Biochem. Pharmacol.* **1993,** *45* (12), 2417-2424.

27. Storr, T.; Merkel, M.; Song-Zhao, G. X.; Scott, L. E.; Green, D. E.; Bowen, M. L.; Thompson, K. H.; Patrick, B. O.; Schugar, H. J.; Orvig, C., Synthesis, Characterization, and Metal Coordinating Ability of Multifunctional Carbohydrate-Containing Compounds for Alzheimer's Therapy. *J. Am. Chem. Soc.* **2007,** *129* (23), 7453–7463.

28. Schugar, H.; Green, D. E.; Bowen, M. L.; Scott, L. E.; Storr, T.; Bohmerle, K.; Thomas, F.; Allen, D. D.; Lockman, P. R.; Merkel, M.; Thompson, K. H.; Orvig, C., Combating Alzheimer's disease with multifunctional molecules designed for metal passivation. *Angewandte Chemie-International Edition* **2007,** *46* (10), 1716-1718.

29. Scott, L. E.; Page, B. D. G.; Patrick, B. O.; Orvig, C., Altering pyridinone N-substituents to optimise activity as potential prodrug for Alzheimer's disease. *Dalton Trans.* **2008**, 6364-6367.

30. Storr, T.; Scott, L. E.; Bowen, M. L.; Green, D. E.; Thompson, K. H.; Schugar, H. J.; Orvig, C., Glycosylated tetrahydrosalens as multifunctional molecules for Alzheimer's therapy. *Dalton Transactions* **2009,** (16), 3034-3043.

31. Storr, T.; Thompson, K. H.; Orvig, C., Design of targeting ligands in medicinal inorganic chemistry *Chem. Soc. Rev.* **2006,** *35*, 534 - 544.

32. Zheng, H.; Blat, D.; Fridkin, M., Novel neuroprotective neurotrophic NAP analogs targeting metal toxicity and oxidative stress: potential candidates for the control of neurodegenerative diseases. *Journal of Neural Transmission* **2006,** *71*, 163-172.

33. Gozes, I.; Lilling, G.; Glazer, R.; Ticher, A.; Ashkenazi, I. E.; Davidson, A.; Rubinraut, S.; Fridkin, M.; Brenneman, D. E., Superactive Lipophilic Peptides Discriminate Multiple Vasoactive Intestinal Peptide Receptors. *Journal of Pharmacology and Experimental Therapeutics* **1995,** *273*, 161-167.

34. Blat, D.; Weiner, L.; Youdim, M. B. H.; Fridkin, M., A Novel Iron-Chelating Derivative of the Neuroprotective Peptide NAPVSIPQ Shows Superior Antioxidant and Antineurodegenerative Capabilities. *J. Med. Chem.* **2008,** *51* (1), 126-134.

35. Zheng, H.; Youdim, M. B. H.; Weiner, L. M.; Fridkin, M., Novel potential neuroprotective agents with both iron chelating and amino acid-based derivatives targeting central nervous system neurons *Biochemical Pharmacology* **2005,** *70* (11), 1642-1652.

36. Ye, Y.; Bloch, S.; Xu, B.; Achilefu, S., Novel near-infrared fluorescent integrin-targeted DFO analogue. *Bioconjugate Chemistry* **2008,** *19* (1), 225-234.

37. Chen, X.; Sievers, E.; Hou, Y.; Park, R.; Tohme, M.; Bart, R.; Bremner, R.; Bading, J. R.; Conti, P. S., Integrin alpha v beta 3-targeted imaging of lung cancer. *Neoplasia* **2005,** *7*, 271-279.

38. Hsu, A. R.; Hou, L. C.; Veeravagu, A.; Greve, J. M.; Vogel, H.; Tse, V.; Chen, X., In Vivo Near-infrared Fluorecence Imaging of Integrin alphavbeta3 in an Orthotopic Glioblastoma Model. *Molecular Imaging and Biology* **2006,** *8* (6), 315-323.

39. Faraji, A. H.; Wipf, P., Nanoparticles in cellular drug delivery. *Bioorganic & Medicinal Chemistry* **2009,** *17* (8), 2950-2962.

40. Cui, Z.; Lockman, P. R.; Atwood, C. S.; Hsu, C.-H.; Gupte, A.; Allen, D. D.; Mumper, R. J., Novel D-penicillamine carrying nanoparticles for metal chelation therapy

in Alzheimer's and other CNS diseases. *European Journal of Pharmaceutics and Biopharmaceutics* **2005,** *59* (2), 263-272.

41. Liu, G.; Men, P.; Harris, P. L. R.; Rolston, R. K.; Perry, G.; Smith, M. A., Nanoparticle iron chelators: A new therapeutic approach in Alzheimer disease and other neurologic disorders associated with trace metal imbalance. *Neuroscience Letters* **2006,** *406* (3), 189-193.

42. Liu, G.; Men, P.; Kudo, W.; Perry, G.; Smith, M. A., Nanoparticle-chelator conjugates as inhibitors of amyloid-[beta] aggregation and neurotoxicity: A novel therapeutic approach for Alzheimer disease. *Neuroscience Letters* **2009,** *455* (3), 187-190.

43. Meijler, M. M.; Arad-Yellin, R.; Cabantchik, Z. I.; Shanzer, A., Synthesis and Evaluation of Iron Chelators with Masked Hydrophilic Moieties *J. Am. Chem. Soc.* **2002,** *124* (43), 12666–12667.

44. Yavin, E.; Kikkiri, R.; Gil, S.; Arad-Yellin, R.; Yavin, E.; Shanzer, A., Synthesis and biological evaluation of lipophilic iron chelators as protective agents from oxidative stress. *Org. Biomol. Chem.* **2005,** *3*, 2685 - 2687.

45. Prousek, J., Fenton chemistry in biology and medicine *Pure and Applied Chemistry* **2007,** *79* (12), 2325-2338.

46. Valko, M.; Morris, H.; Cronin, M. T. D., Metals, Toxicity and Oxidative Stress. *Curr. Med. Chem.* **2005,** *12*, 1161-1208.

47. Chiueh, C. C., Iron overload, oxidative stress, and axonal dystrophy in brain disorders. *Pediatric Neurology* **2001,** *25* (2), 138-147.

48. Ke, Y.; Qian, Z. M., Iron misregulation in the brain: a primary cause of neurodegenerative disorders. *Lancet Neurology* **2003,** *2* (4), 246-253.

49. Rouault, T. A., Iron on the brain. *Nature Genetics* **2001,** *28* (4), 299-300.

50. Charkoudian, L. K.; Pham, D. M.; Franz, K. J., A Pro-Chelator Triggered by Hydrogen Peroxide Inhibits Iron-Promoted Hydroxyl Radical Formation. *J. Am. Chem. Soc.* **2006,** *128* (38), 12424-12425.

51. Charkoudian, L. K., Pham, D. M., Kwon, A. M., Vangeloff, A. D., Franz, K. J., Modifications of Boronic Ester Pro-Chelators Triggered by Hydrogen Peroxide Tune Reactivity to Inhibit Metal-Promoted Oxidative Stress. *Dalton Trans.* **2007**, 5031-5042.

52. Charkoudian, L. K., Dentchev, T., Lukinova, N., Wolkow, N. Dunaief, J. L., Franz, K. J., Iron prochelator BSIH protects retinal pigment epithelial cells against cell death induced by hydrogen peroxide. *Journal of Inorganic Biochemistry* **2008,** *102*, 2130-2135.

53. Yiakouvaki, A.; Savovic, J.; Al-Qenaei, A.; Dowden, J.; Pourzand, C., Caged-Iron Chelators a Novel Approach towards Protecting Skin Cells against UVA-Induced Necrotic Cell Death. *Journal of Investigative Dermatology* **2006,** *126*, 2287–2295.

54. Pourzand, C.; Watkin, R. D.; Brown, J. E.; Tyrrell, R. M., Ultraviolet A radiation induces immediate release of iron in human primary skin fibroblasts: The role of ferritin. *Proceedings of the National Academy of Sciences of the United States of America* **1999,** *96* (12), 6751-6756.

55. Galey, J.-B.; Dumats, J.; Beck, I.; Fernandez, B.; Hocquaux, M., N,N'-Bis-Dibenzyl Ethylenediaminediacetic Acid (Dbed): a Site-Specific Hydroxyl Radical Scavenger Acting as an ,ÄúOxidative Stress Activatable,Âù Iron Chelator In Vitro. *Free Radical Research* **1995,** *22* (1), 67 - 86.

56. Serratrice, G.; Galey, J. B.; Saint Aman, E.; Dumats, J., Iron(III) Complexation by New Aminocarboxylate Chelators - Thermodynamic and Kinetic Studies. *European Journal of Inorganic Chemistry* **2001,** (2), 471-479.

57. Galey, J.-B.; Destrée, O.; Dumats, J.; Génard, S.; Tachon, P., Protection against Oxidative Damage by Iron Chelators: Effect of Lipophilic Analogues and Prodrugs of N,N'-Bis(3,4,5-trimethoxybenzyl)ethylenediamine- N,N'-diacetic Acid (OR10141). *J. Med. Chem.* **2000,** *43* (7), 1418–1421.

58. Galey, J.-B.; Dumats, J.; Genard, S.; Destree, O.; Pichaud, P.; Cctroux, P.; Marrot, L.; Beck, I.; Fernandez, B.; Barre, G.; Seite, M.; Hussler, G.; Hocquaux, M., N,N'-bis-(3,4,5-trimethoxybenzyl) ethylenediamine N,N'-diacetic acid as a new iron chelator with potential medicinal applications against oxidative stress. *Biochemical Pharmacology* **1996,** *51* (2), 103-115.

59. Naughton, D. P.; Grootveld, M., EDTA Bis-(ethyl phenylalaninate): A Novel Transition Metal-Ion Chelating Hydroxyl Radical Scavenger with a Potential Anti-inflammatory Role. *Bioorganic & Medicinal Chemistry Letters* **2001,** *11*, 2573-2575.

60. Di Stefano, A.; Sozio, P.; Iannitelli, A.; Cerasa, L. S., New drug delivery strategies for improved Parkinson's disease therapy. *Expert Opinion on Drug Delivery* **2009,** *6* (4), 389-404.

61. Di Stefano, A.; Sozio, P.; Cerasa, L. S., Antiparkinson Prodrugs. *Molecules* **2008,** *13*, 46-68.

62. Di Stefano, A.; Sozio, P.; Cocco, A.; Iannitelli, A.; Santucci, E.; Costa, M.; Pecci, L.; Nasuti, C.; Cantalamessa, F.; Pinnen, F., L-Dopa- and Dopamine-(R)-alpha-Lipoic Acid Conjugates as Multifunctional Codrugs with Antioxidant Properties. *Journal of Medicinal Chemistry* **2006,** *49* (4), 1486-1493.

63. Packer, L.; Tritschler, H. J.; Wessel, K., Neuroprotection by the Metabolic Antioxidant -Lipoic Acid. *Free Radical Biology and Medicine* **1997,** *22* (1-2), 359-378.

64. Suh, J. H.; Ben-Zhan, Z.; DeSzoeke, E.; Frei, B.; Hagen, T. M., Dihydrolipoic acid lowers the redox activity of transition metal ions but does not remove them from the active site of enzymes. *Redox Report* **2004,** *9* (1), 57-61.

65. Bebbington, D.; Monck, N. J. T.; Gaur, S.; Palmer, A. M.; Benwell, K.; Harvey, V.; Malcolm, C. S.; Porter, R. H. P., 3,5-Disubstituted-4-hydroxyphenyls Linked to 3-

Hydroxy-2-methyl- 4(1H)-pyridinone: Potent Inhibitors of Lipid Peroxidation and Cell Toxicity. *Journal of Medicinal Chemistry* **2000,** *43* (15), 2779-2782.

66. Bebbington, D.; Dawson, C. E.; Gaur, S.; Spencer, J., Prodrug and covalent linker strategies for the solubilization of dual-Action antioxidants/Iron chelators. *Bioorganic & Medicinal Chemistry Letters* **2002,** *12* (22), 3297-3300.

67. Rauk, A., Why is the amyloid beta peptide of Alzheimer's disease neurotoxic? *Dalton Trans.* **2008**, 1273-1282.

68. Bush, A. I., The metallobiology of Alzheimer's disease. *Trends in Neurosciences* **2003,** *26* (4), 207-214.

69. Adlard, P. A.; Cherny, R. A.; Finkelstein, D. I.; Gautier, E.; Robb, E.; Cortes, M.; Volitakis, I.; Liu, X.; Smith, J. P.; Perez, K.; Laughton, K.; Li, Q.-X.; Charman, S. A.; Nicolazzo, J. A.; Wilkins, S.; Deleva, K.; Lynch, T.; Kok, G.; Ritchie, C. W.; Tanzi, R. E.; Cappai, R.; Masters, C. L.; Barnham, K. J.; Bush, A. I., Rapid Restoration of Cognition in Alzheimer's Transgenic Mice with 8-Hydroxy Quinoline Analogs Is Associated with Decreased Interstitial A[beta]. *Neuron* **2008,** *59* (1), 43-55.

70. Ritchie, C. W.; Bush, A. I.; Mackinnon, A.; Macfarlane, S.; Mastwyk, M.; MacGregor, L.; Kiers, L.; Cherny, R.; Li, Q.-X.; Tammer, A.; Carrington, D.; Mavros, C.; Volitakis, I.; Xilinas, M.; Ames, D.; Davis, S.; Beyreuther, K.; Tanzi, R. E.; Masters, C. L., Metal-Protein Attenuation With Iodochlorhydroxyquin (Clioquinol) Targeting A{beta} Amyloid Deposition and Toxicity in Alzheimer Disease: A Pilot Phase 2 Clinical Trial. *Arch Neurol* **2003,** *60* (12), 1685-1691.

71. Dedeoglu, A.; Cormier, K.; Payton, S.; Tseitlin, K. A.; Kremsky, J. N.; Lai, L.; Li, X.; Moir, R. D.; Tanzi, R. E.; Bush, A. I.; Kowall, N. W.; Rogers, J. T.; Huang, X., Preliminary Studies of a Novel Bifunctional Metal Chelator Targeting Alzheimer's Amyloidogonesis. *Experimental Gerontology* **2004,** *39*, 1641-1649.

72. Rodriguez-Rodriguez, C.; Sanchez de Groot, N.; Rimola, A.; Alvarez-Larena, A.; Lloveras, V.; Vidal-Gancedo, J.; Ventura, S.; Vendrell, J.; Sodupe, M.; Gonzalez-Duarte, P., Design, Selection, and Characterization of Thioflavin-Based Intercalation Compounds with Metal Chelating Properties for Application in Alzheimer’s Disease. *Journal of the American Chemical Society* **2009,** *131* (4), 1436-1451.

73. Opazo, C.; Huang, X.; Cherny, R. A.; Moir, R. D.; Roher, A. E.; White, A. R.; Cappai, R.; Masters, C. L.; Tanzi, R. E.; Inestrosa, N. C.; Bush, A. I., Metalloenzyme-like Activity of Alzheimer's Disease beta -Amyloid. Cu-Dependent Catalytic Conversion of Dopamine, Cholesterol, and Biological Reducing Agents to Neurotoxic H2O2. *Journal of Biological Chemistry* **2002,** *277* (43), 40302-40308.

74. Tabner, B. J.; El-Agnaf, O. M. A.; Turnbull, S.; German, M. J.; Paleologou, K. E.; Hayashi, Y.; Cooper, L. J.; Fullwood, N. J.; Allsop, D., Hydrogen Peroxide Is Generated during the Very Early Stages of Aggregation of the Amyloid Peptides Implicated in Alzheimer Disease and Familial British Dementia. *Journal of Biological Chemistry* **2005,** *280* (43), 35789-35792.

75. Dickens, M. G.; Franz, K. J., A Prochelator Activated by Hydrogen Peroxide Prevents Metal-Induced Amyloid Beta Aggregation. *submitted for publication* **2009**.

76. Suh, J.; Yoo, S.; Kim, M.; Jeong, K.; Ahn, J. Y.; Kim, M. S.; Chae, P. S.; Lee, T. Y.; Lee, J.; Jang, Y. A.; Ko, E. H., Cleavage agents for soluble oligomers of amyloid beta peptides. *Angewandte Chemie-International Edition* **2007,** *46* (37), 7064-7067.

77. Suh, J.; Chei, W. S., Metal complexes as artificial proteases: toward catalytic drugs. *Current Opinion in Chemical Biology* **2008,** *12* (2), 207-213.

78. Wu, W.; Lei, P.; Liu, Q.; Hu, J.; Gunn, A. P.; Chen, M.; Rui, Y.; Su, X.; Xie, Z.; Zhao, Y.; Bush, A. I.; Li, Y., Sequestration of Copper from {beta}-Amyloid Promotes Selective Lysis by Cyclen-Hybrid Cleavage Agents. *Journal of Biological Chemistry* **2008,** *283* (46), 31657-31664.

79. Youdim, M. B. H.; Fridkin, M.; Zheng, H., Novel bifunctional drugs targeting monoamine oxidase inhibition and iron chelation as an approach to neuroprotection in Parkinson's disease and other neurodegenerative diseases. *Journal of Neural Transmission* **2004,** *111* (10-11), 1455-1471.

80. Zheng, H.; Gal, S.; Weiner, L. M.; Bar-Am, O.; Warshawsky, A.; Fridkin, M.; Youdim, M. B. H., Novel multifunctional neuroprotective iron chelator-monoamine oxidase inhibitor drugs for neurodegenerative diseases: in vitro studies on antioxidant activity, prevention of lipid peroxide formation and monoamine oxidase inhibition *Journal of Neurochemistry* **2005,** *95*, 68-78.

81. Youdim, M. B. H., The Path from Anti Parkinson Drug Selegiline and Rasagiline to Multifunctional Neuroprotective Anti Alzheimer Drugs Ladostigil and M30. *Current Alzheimer Research* **2006,** *3* (5), 541-550.

82. Zheng, H.; Weiner, L. M.; Bar-Am, O.; Epsztejn, S.; Cabantchik, Z. I.; Warshawsky, A.; Youdim, M. B. H.; Fridkin, M., Design, synthesis, and evaluation of novel bifunctional iron-chelators as potential agents for neuroprotection in Alzheimer's, Parkinson's, and other neurodegenerative diseases *Bioorganic & Medicinal Chemistry Letters* **2005,** *13* (3), 773-783.

83. Avramovich-Tirosh, Y.; Amit, T.; Bar-Am, O.; Zheng, H.; Fridkin, M.; Youdim, M. B. H., Therapeutic targets and potential of the novel brain- permeable multifunctional iron chelator-monoamine oxidase inhibitor drug, M-30, for the treatment of Alzheimer's disease *Journal of Neurochemistry* **2007,** *100* (2), 490-502.

84. Avramovich-Tirosh, Y.; Rezrlichenko, D.; Amit, T.; Zheng, H.; Fridkin, M.; Weinreb, O.; Mandel, S.; Youdim, M. B. H., Neurorescue activity, APP regulation and amyloid-beta peptide reduction by novel multi-functional brain permeable iron-chelating- antioxidants, m-30 and green tea polyphenol, EGCG. *Current Alzheimer Research* **2007,** *4* (4), 403-411.

85. Mandel, S.; Amit, T.; Bar-Am, O.; Youdim, M. B. H., Iron dysregulation in Alzheimer's disease: Multimodal brain permeable iron chelating drugs, possessing

neuroprotective-neurorescue and amyloid precursor protein-processing regulatory activities as therapeutic agents. *Progress in Neurobiology* **2007,** *82* (6), 348-360.

86. Cavalli, A.; Bolognesi, M. L.; Minarini, A.; Rosini, M.; Tumiatti, V.; Recanatini, M.; Melchiorre, C., Multi-target-Directed Ligands to Combat Neurodegenerative Diseases. *Journal of Medicinal Chemistry* **2008,** *51* (3), 347-372.

87. Bolognesi, M. L.; Cavalli, A.; Valgimigli, L.; Bartolini, M.; Rosini, M.; Andrisano, V.; Recanatini, M.; Melchiorre, C., Multi-Target-Directed Drug Design Strategy: From a Dual Binding Site Acetylcholinesterase Inhibitor to a Trifunctional Compound against Alzheimer's Disease. *J. Med. Chem.* **2007,** *50* (26), 6446-6449.

88. Pang, Y.-P.; Quiram, P.; Jelacic, T.; Hong, F.; Brimijoin, S., Highly Potent, Selective, and Low Cost Bis-tetrahydroaminacrine Inhibitors of Acetylcholinesterase. *Journal of Biological Chemistry* **1996,** *271* (39), 23646- 23649.

89. Zheng, H.; Youdim, M. B. H.; Fridkin, M., Site-Activated Multifunctional Chelator with Acetylcholinesterase and Neuroprotective,àíNeurorestorative Moieties for Alzheimer,Äôs Therapy. *Journal of Medicinal Chemistry* **2009,** *52* (14), 4095-4098.

90. Ba, L. A.; Doering, M.; Burkholz, T.; Jacob, C., Metal trafficking: from maintaining the metal homeostasis to future drug design. *Metallomics* **2009,** *1* (4), 292-311.

92. Galey, J. B. D., O.; Dumats, J.; Génard, S.; Tachon, P., Protection against Oxidative Damage by Iron Chelators: Effect of Lipophilic Analogues and Prodrugs of N,N'-Bis(3,4,5-trimethoxybenzyl)ethylenediamine- N,N'-diacetic Acid (OR10141). *J. Med. Chem.* **2000,** *43* (7), 1418–1421.

93. Nick, H., Iron Chelation, quo vadis? *Current Opinion in Chemical Biology* **2007,** *11*, 419-423.

94. Ponka, P., Borova, J., Neuwirt, J., Fuchs, O, Mobilization of iron from reticulocytes. Identification of pyridoxal isonicotinoyl hydrazone as a new iron chelating agent. *Febs Lett* **1979,** *97*, 317-321.

95. Edward, J. T., Gauthier, M., Chubb, F. L., Ponka, Synthesis of new acylhydrazones as iron-chelating compounds. *P. J. Chem. Eng. Data* **1988,** *33*, 538- 540.

96. KovarÌkov·, P.; V·vrov·, K.; Tomalov·, K.; Schˆngut, M.; Hruskov·, K.; Haskov·, P.; Klimes, J., HPLC-DAD and MS/MS analysis of novel drug candidates from the group of aromatic hydrazones revealing the presence of geometric isomers. *Journal of Pharmaceutical and Biomedical Analysis* **2008,** *48* (2), 295-302.

97. Richardson, D. R.; Bernhardt, P. V., Crystal and molecular structure of 2-hydroxy-1-naphthaldehyde isonicotinoyl hydrazone (NIH) and its iron(III) complex: an iron chelator with anti-tumour activity. *J. Biol. Inorg. Chem.* **1999,** *4* (3), 266-273.

98. Bastian, R.; Weberling, R.; Palilla, F., Determination of iron by ultraviolet spectrophotometry. *Anal. Chem.* **1956,** *28* (4), 459–462.

99. Perrin, D. D.; Dempsey, B., *Buffers for pH and Metal ion and control*. Chapman and Hall: London, 1922.

100. Albrecht-Gary, A.-M.; Crumbliss, A. L., Coordination chemistry of siderophores: Thermodynamics and kinetics of iron chelation and release. In *Metal Ions in Biological Systems*, Sigel, A.; Sigel, H., Eds. Marcel Dekker: New York, 1973; Vol. 35, pp 239–327.

101. Crumbliss, A. L.; Garrison, M. J., A Comparison of Some Aspects of the Aqueous Coordination Chemistry of Aluminum(III) and Iron(III). *Comments Inorg. Chem.* **1988,** *8* (Nos. 1 & 2), 1-26.

102. Martell, A. E.; Smith, R. M., *Critical Stablity Constants*. Plenum Press: New York and London, Vol. 1.